HHS Public Access

Author manuscript

Nature. Author manuscript; available in PMC 2024 June 06.

Published in final edited form as:

Nature. 2024 June ; 630(8015): 237–246. doi:10.1038/s41586-024-07403-2.

Structural pharmacology and therapeutic potential of 5-methoxytryptamines

Audrey L. Warren[1,5], **David Lankri**[2,5], **Michael J. Cunningham**[2], **Inis C. Serrano**[2], **Lyonna F. Parise**[3], **Andrew C. Kruegel**[2], **Priscilla Duggan**[2], **Gregory Zilberg**[4], **Michael J. Capper**[1], **Vaclav Havel**[2], **Scott J. Russo**[3], **Dalibor Sames**[2,4,✉], **Daniel Wacker**[1,3,✉]

[1]Department of Pharmacological Sciences, Icahn School of Medicine at Mount Sinai, New York, NY, USA

[2]Department of Chemistry, Columbia University, New York, NY, USA

[3]Department of Neuroscience, Icahn School of Medicine at Mount Sinai, New York, NY, USA

[4]Zuckerman Institute of Mind, Brain, Behavior, Columbia University, New York, NY, USA

[5]These authors contributed equally: Audrey L. Warren, David Lankri

Abstract

Psychedelic substances such as lysergic acid diethylamide (LSD) and psilocybin show potential for the treatment of various neuropsychiatric disorders[1–3]. These compounds are thought to mediate their hallucinogenic and therapeutic effects through the serotonin (5-hydroxytryptamine (5-HT)) receptor 5-HT_{2A} (ref. 4). However, 5-HT_{1A} also plays a part in the behavioural effects of tryptamine hallucinogens[5], particularly 5-methoxy-*N,N*-dimethyltryptamine (5-MeO-DMT), a psychedelic found in the toxin of Colorado River toads[6]. Although 5-HT_{1A} is a validated therapeutic target[7,8], little is known about how psychedelics engage 5-HT_{1A} and which effects are mediated by this receptor. Here we map the molecular underpinnings of 5-MeO-DMT pharmacology through five cryogenic electron microscopy (cryo-EM) structures of

✉**Correspondence and requests for materials** should be addressed to Dalibor Sames or Daniel Wacker. ds584@columbia.edu; daniel.wacker@mssm.edu.

Author contributions D.S., A.C.K, M.J. Cunningham and D.L. conceived and initiated the project. A.L.W. designed experiments, expressed and purified protein for grid freezing, collected data, refined structures with help from M.J. Capper, performed signalling and uptake assays, and co-wrote the manuscript. D.L. designed, synthesized, purified and characterized compounds with assistance from V.H., and co-wrote the manuscript. M.J. Cunningham designed, synthesized, purified and characterized compounds. D.L., V.H. and D.S. designed and supervised the pharmacokinetics study. L.F.P. performed the chronic SD stress assay and subsequent behavioural analyses supervised by S.J.R. I.C.S. designed and performed in vivo pharmacology assays, including the open-field and HTR assays, with assistance from P.D. G.Z. prepared grids for structure determination and assisted with data collection. D.S. and D.W. conceptualized the overall project and designed experiments, analysed the data, supervised the project and management, and wrote the manuscript.

Competing interests The authors declare the following competing financial interests: D.S. and A.C.K. are co-founders of Gilgamesh Pharmaceuticals and Kures. M.J. Cunningham is a co-founder of Gilgamesh Pharmaceuticals. A.L.W., D.L., I.C.S., L.F.P., S.J.R., D.S. and D.W. are inventors on a patent application related to the featured compound class. D.W. has consulted for Otsuka Pharmaceutical, Longboard Pharmaceuticals and Ocean Bio on the design of psychedelic-based therapeutics. None of the companies listed herein contributed to the funding or experimental design. All other authors declare no competing interests.

Supplementary information The online version contains supplementary material available at https://doi.org/10.1038/s41586-024-07403-2.

Peer review information *Nature* thanks the anonymous reviewers for their contribution to the peer review of this work. Peer reviewer reports are available.

5-HT_{1A}, systematic medicinal chemistry, receptor mutagenesis and mouse behaviour. Structure–activity relationship analyses of 5-methoxytryptamines at both 5-HT_{1A} and 5-HT_{2A} enable the characterization of molecular determinants of 5-HT_{1A} signalling potency, efficacy and selectivity. Moreover, we contrast the structural interactions and in vitro pharmacology of 5-MeO-DMT and analogues to the pan-serotonergic agonist LSD and clinically used 5-HT_{1A} agonists. We show that a 5-HT_{1A}-selective 5-MeO-DMT analogue is devoid of hallucinogenic-like effects while retaining anxiolytic-like and antidepressant-like activity in socially defeated animals. Our studies uncover molecular aspects of 5-HT_{1A}-targeted psychedelics and therapeutics, which may facilitate the future development of new medications for neuropsychiatric disorders.

Recent scientific inquiry has demonstrated that serotonergic psychedelics such as psilocybin and LSD have both rapid and long-lasting anxiolytic and antidepressant effects[3]. Although the mind-altering, psychedelic effects of these compounds have been ascribed to actions at 5-HT_{2A} receptors, studies indicate that other 5-HT receptors have a modulatory role. The complex animal behavioural effects of the less-studied hallucinogen 5-MeO-DMT, found in the poison of the Colorado River toad (*Incilius alvarius*)[6], are particularly reliant on the actions of the drug at 5-HT_{1A} receptors. The discriminatory stimulus of 5-MeO-DMT and its effects on exploratory behaviours and sedation are largely driven by 5-HT_{1A} agonist activity in vivo[5,9]. Epidemiological surveys, which capture alternative medical uses of 5-MeO-DMT, indicate that 5-MeO-DMT generates a rapid and sustained reduction in depression and anxiety symptoms, as well as induction of meaningful and spiritually significant experiences[10]. 5-MeO-DMT is also clinically used in combination with the oneirogen ibogaine outside the United States. A recent survey of US Special Operation Forces veterans highlighted the therapeutic promise of this compound in the treatment of post-traumatic stress disorder (suicidal ideation and cognitive impairment), depression and anxiety[2]. 5-MeO-DMT is currently in development as a therapeutic for a range of indications, including depression, substance use disorders and neurological disorders[11]. Although based largely on open-label trials and naturalistic surveys, the existing evidence suggests that 5-MeO-DMT produces rapid and strong effects across neuropsychiatric diagnostic indications. Given that 5-HT_{1A} is the primary target of approved anxiolytic and antidepressant medications, such as buspirone (BuSpar)[8] and vilazodone (Viibryd)[12], this receptor may contribute to the reported therapeutic effects of 5-MeO-DMT.

Although much has recently been uncovered about the molecular mechanisms of LSD and other psychedelics at 5-HT_{2A} receptors[13,14], little is known about how 5-MeO-DMT, related tryptamines and classical psychedelics bind to and signal through 5-HT_{1A}. Most research and development of new probes of psychedelics have focused on 5-HT_{2A} receptors[15,16], whereas notably less effort has been dedicated to investigating the role of other 5-HT receptors in the polypharmacology of these compounds. This is despite the proposed complementary roles of 5-HT_{1A} and 5-HT_{2A} in moderating anxiety and stress[17], which are some of the major areas for potential psychedelic-based therapies. Here we report a detailed structural and functional exploration of the mechanisms by which classical psychedelics, 5-methoxytryptamines (5-MeO-tryptamines) and prescription drugs bind to and activate 5-HT_{1A} at the molecular and atomic level. We also report on 5-HT_{1A}-selective tryptamines in a mouse model of depression, highlighting the potential of new tryptamine-

based 5-HT_{1A} medications. Our studies provide crucial insights into an understudied class of psychedelics and related compounds that may facilitate the development of new neuropsychiatric therapeutics that target 5-HT_{1A}.

Psychedelics acting at 5-HT_{1A} and 5-HT_{2A}

To compare the actions of psychedelics at both 5-HT_{1A} and 5-HT_{2A}, we determined the signalling activities at both receptors using bioluminescence resonance energy transfer (BRET) G_{i1} and G_q activation reporters, respectively[14,18] (Fig. 1a). In line with previous reports[19,20] most psychedelic drugs tested at 5-HT_{2A} showed partial agonism, ranging from efficacies near 50% of that of serotonin for psilocin (the active metabolite of psilocybin) to nearly 100% as seen for mescalline (the main psychoactive alkaloid in peyote). *N,N*-dimethyltryptamine (DMT; the psychedelic compound in ayahuasca), psilocin and mescaline were more potent at 5-HT_{2A}, whereas LSD and 5-MeO-DMT were effectively equipotent at 5-HT_{1A} and 5-HT_{2A} (Fig. 1a). Despite the variation in selectivity and potency, the tryptamine psychedelics were full or near-full agonists of 5-HT_{1A}-mediated G protein signalling in our assays compared with serotonin (Fig. 1a and Supplementary Table 1). These findings validate the potency and efficacy of both LSD and 5-MeO-DMT at 5-HT_{1A}, complementing previous studies that have demonstrated the importance of 5-HT_{1A} in the in vivo pharmacology of both drugs[5,21].

Structures of psychedelic-bound 5-HT_{1A}

To elucidate the structural basis of how 5-MeO-DMT and LSD activate 5-HT_{1A}, we determined cryo-EM structures of drug-bound 5-HT_{1A}–G_i signalling complexes (Fig. 1b and Extended Data Fig. 1a). We used previously reported receptor and G protein constructs that we[13] and others[22] have used to determine 5-HT_{2A} and 5-HT_{1A} structures (see Methods for details). In brief, for 5-HT_{1A}, we replaced the first 24 residues with BRIL to facilitate expression and introduced a stabilizing $L125^{3.41}W$ mutation (superscript numbers denote Ballesteros–Weinstein numbering[23]). For the heterotrimeric G protein, we co-expressed $G\beta_1$ with a $G\gamma_2$–$G\alpha_{i1}$ fusion[13] containing stabilizing mutations[22].

The cryo-EM structures of 5-MeO-DMT-bound and LSD-bound 5-HT_{1A}–G_i signalling complexes were obtained at global nominal resolutions of 2.79 Å and 2.64 Å, respectively (Fig. 1b, Extended Data Fig. 1 and Extended Data Table 1). Our structures enabled us to unambiguously resolve backbones and side chains, elucidate sterols and lipids, and characterize drug–receptor interactions in molecular detail (Fig. 1b and Extended Data Fig. 2b). The structures displayed conserved features of active-state G protein-coupled receptors, such as an outward-rotated receptor TM6 and the carboxy-terminal α5 helix of the $G\alpha_{i1}$ protein bound to the cytoplasmic transducer site of 5-HT_{1A} receptors[22,24]. We observed a similar overall receptor conformation compared with previous 5-HT_{1A} structures[22], with a root mean square deviation of 0.596 Å (Extended Data Fig. 2a), and we were able to elucidate additional 5-HT_{1A} residues such as a complete extracellular loop 2 (EL2). Notably, our structures uncovered distinct drug–receptor interactions in the orthosteric binding pocket (OBP) that may drive differences in drug pharmacology. Primarily anchored by a conserved ionic interaction with $D116^{3.32}$, 5-MeO-DMT and LSD bind 0.8 Å deeper

in the pocket (measured from the indole nitrogen to the oxygen of T121$^{3.37}$) compared with the structurally similar serotonin[22] (Fig. 1b). In addition, we observed a hydrogen bond between the indole nitrogen of the drugs and T121$^{3.37}$ at the bottom of the 5-HT$_{1A}$-binding pocket, which is not observed for serotonin. This leads to a slight 8.5° rotation around an axis formed by the amine-D116$^{3.32}$ bond for 5-MeO-DMT, a feature previously observed for ergoline compounds such as LSD at other 5-HT receptors[14,25]. Indeed, LSD displays a 15.4° rotation towards the receptor core compared with the poses observed in our previous LSD-bound 5-HT$_{2B}$ and 5-HT$_{2A}$ structures[13,14], forming a similar interaction with T121$^{3.37}$ as observed for 5-MeO-DMT (Fig. 1b and Extended Data Fig. 2e). Starting from the conserved interaction with D116$^{3.32}$, the diethylamide substituent of LSD extends towards the extracellular site forming hydrophobic interactions with I189^{EL2} in EL2. A similar interaction with L229^{EL2} of 5-HT$_{2A}$ was suggested to be crucial for the slow binding kinetics and distinct pharmacological profile of LSD[13,14]. Overall, we observed that the diethylamide substituent of LSD is accommodated 1 Å closer to TM3 (measured as the distance to the Cα of I$^{3.29}$) with one of the ethyl groups of LSD sandwiched between the side chains of F112$^{3.28}$ and I113$^{3.29}$ (Extended Data Fig. 2e). This configuration is different from that observed in LSD-bound 5-HT$_{2A}$, which is intriguing because the configuration of the ethyl groups of LSD seems to be pivotal for its pharmacology and psychedelic effects in vivo[14,26].

Our structural data revealed that LSD adopts distinct binding modes at 5-HT$_{1A}$ and 5-HT$_{2A}$. Moreover, 5-MeO-DMT assumes a different binding pose from related serotonin at 5-HT$_{1A}$. However, it is unclear whether these differences are driven by the methylation of the amine, the methylation of the hydroxyl group or both.

Structure–activity relationship of 5-MeO-tryptamines at 5-HT$_{1A}$

Using 5-MeO-DMT as the starting point, we set out to systematically examine the structure–activity relationship (SAR) of 5-MeO-tryptamines and to uncover determinants of potency and selectivity at 5-HT$_{1A}$ and 5-HT$_{2A}$. The compounds were synthesized using indoles with the desired substitution and the oxalylation–amidation–reduction sequence[27] to prepare the corresponding tryptamine analogues (Extended Data Fig. 3 and Supplementary Data 1).

As the first structural variable, we investigated the effect of different amine modifications, including comparisons of acyclic and cyclic amines on 5-HT$_{1A}$ and 5-HT$_{2A}$ signalling (Fig. 2 and Supplementary Table 1). Several of these compounds are known as ‘designer tryptamines’, with anecdotal reports of psychedelic activity in humans (Supplementary Table 2), including 5-methoxy-*N*,*N*-dipropyl-tryptamine (5-MeO-DPT), 5-methoxy-*N*-methyl, *N*-isopropyl-tryptamine (5-MeO-MiPT) and 5-methoxy-*N*,*N*-pyrrolidinyl-tryptamine (5-MeO-PyrT)[28,29]. Extension of the methyl groups of 5-MeO-DMT (G_i BRET half-maximum effective concentration (EC_{50}) = 25.6 nM) to one ethyl group (5-MeO-MET; G_i BRET EC_{50} = 25.9 nM) or two ethyl groups (5-MeO-DET; G_i BRET EC_{50} = 37.1 nM) only marginally affected 5-HT$_{1A}$ potency while retaining full efficacy, with similarly small effects at 5-HT$_{2A}$ (Supplementary Table 1). By contrast, a cyclic pyrrolidine substituent increased potency at 5-HT$_{1A}$ by about 12-fold (5-MeO-PyrT; G_i BRET EC_{50} = 2.1 nM) and decreased 5-HT$_{2A}$ potency by about 3-fold relative to 5-MeO-DMT. Cyclization of the

amine moiety alone resulted in an approximately 38-fold increase in 5-HT_{1A} > 5-HT_{2A} selectivity. Next, we modestly decreased the steric demand of the pyrrolidine by removing two C-H bonds and installing a π bond. This change led to a further increase of around eightfold in potency at 5-HT_{1A} (5-MeO-3-PyrrolineT; G_i BRET EC_{50} = 0.3 nM). By contrast, increasing the ring size to a six-membered piperidine (5-MeO-PipT; G_i BRET EC_{50} = 88.5 nM) led to an approximate 42-fold loss of potency relative to 5-MeO-PyrT, which indicated a sensitivity to steric bulk at 5-HT_{1A} (Fig. 2b). Further elaboration to isoquinuclidine-containing tryptamines related to ibogaine led to a complete loss of 5-HT_{1A} activity (Supplementary Table 1 and Extended Data Fig. 3).

As the second structural variable, we tested different modifications of the indole nucleus. We mapped the SAR of several positions of the indole to investigate the specificity of the 5-MeO-DMT core for potent 5-HT_{1A} activity (Fig. 2 and Supplementary Table 1). On the basis of previous studies showing that indole fluorination strongly affects 5-HT_1 and 5-HT_2 binding affinities[30,31], we introduced fluorine in the 4-position of 5-MeO-DMT (4-F,5-MeO-DMT). This modification led to a 14-fold increase in signalling potency at 5-HT_{1A} and a 3-fold decrease in potency at 5-HT_{2A}. This trend was consistent across different analogues, whereby 4-fluorination caused an approximately tenfold increase in potency at 5-HT_{1A} and about fivefold potency decrease at 5-HT_{2A} (except for 5-MeO-3-PyrrolineT). Consequently, combining amine cyclization and 4-fluorination generated highly potent 5-HT_{1A} compounds, such as 4-F,5-MeO-PyrT (G_i BRET EC_{50} = 370 pM) and 4-F,5-MeO-3-PyrrolineT (G_i BRET EC_{50} = 220 pM). 4-F,5-MeO-PyrT was the more selective compound, with a greater than 800-fold selectivity for 5-HT_{1A} > 5-HT_{2A}, an effect driven by both an increased potency at 5-HT_{1A} and a decreased potency at 5-HT_{2A} (Fig. 2).

Amine alkylation and 5-HT_{1A} activity

To investigate the structural determinants of the observed SAR effects, we determined a cryo-EM structure of the 5-HT_{1A} signalling complex bound to 4-F,5-MeO-PyrT at a global resolution of 2.85 Å (Fig. 3, Extended Data Fig. 4 and Extended Data Table 1). Ligand modifications did not alter the binding pose, and we observed almost indistinguishable interactions with $D116^{3.32}$ and $T121^{3.37}$ compared with 5-MeO-DMT but distinct from serotonin (Figs. 1 and 3 and Extended Data Fig. 4). Similar to the methyl groups in 5-MeO-DMT, the pyrrolidyl substituent of 4-F,5-MeO-PyrT is wedged between $F361^{6.51}$, $Y390^{7.43}$ and $N386^{7.39}$ (Fig. 3 and Extended Data Fig. 4c).

We first probed this interaction by mutating the conserved $F361^{6.51}$ to leucine and successively smaller hydrophobic side chains. Tryptamines with smaller or no amine substituents, such as 5-MeO-DMT and serotonin, showed greater loss of 5-HT_{1A} potency than 4-F,5-MeO-PyrT (Extended Data Fig. 4d and Supplementary Table 3). These results indicate that $F361^{6.51}$ not only stabilizes the overall tryptamine scaffold, as shown in previous studies[32], but also plays a key part in the potencies of different amine substitutions. We then investigated the interaction of $N386^{7.39}$ by mutating it to the corresponding valine found at this position in 5-HT_{2A}. This modification led to a strong reduction in 5-HT_{1A} potency for 5-MeO-PyrT but not 5-MeO-DMT. Conversely, the $V366N^{7.39}$ mutation in 5-HT_{2A} resulted in a small increase in potency only with cyclic amines. Notably, this mutation

also led to an increase in signalling efficacy at 5-HT_{2A} across N-substituted tryptamines, including LSD. These findings highlight the importance of interactions with residues in position 7.39 for the activities of tryptamine ligands (Fig. 3). Our results also show that the residues F361$^{6.51}$, Y390$^{7.43}$ and N386$^{7.39}$ create a milieu that accommodates small amine rings that in turn leads to increased signalling potencies of these compounds.

Indole substitution and 5-HT_{1A} activity

Our SAR results confirmed that the introduction of fluorine in the 4-position or different groups in the 5-position of the indole nucleus substantially increases the signalling potency at 5-HT_{1A} and affects 5-HT_{1A} > 5-HT_{2A} selectivity (Fig. 2 and Supplementary Table 1). To investigate the mechanistic basis of these differences, we focused on A365$^{6.55}$, as this alanine is unique to 5-HT_{1A} among 5-HT receptors and is situated in proximity to the 4-indole and 5-indole substituents. We therefore mutated A365$^{6.55}$ to the corresponding asparagine found at this position in 5-HT_{2A}. We observed a reduction in potency of all examined tryptamines, including fluorinated analogues, with the largest decrease of about 18-fold for 5-OH-DMT (bufotenine) (Supplementary Table 3). The A365$^{6.55}$ of 5-HT_{1A} is therefore important for the high potency of 5-substituted tryptamines, an effect probably due to its ability to accommodate groups with various chemical properties. Meanwhile, specific interactions with A365$^{6.55}$ are not responsible for increases in potency of fluorinated tryptamines, which are probably driven by the changes in electron density distribution in the fluorinated compounds and the resulting interactions with larger surfaces of the receptor.

Conversely, the N343$^{6.55}$ mutation in 5-HT_{2A} to the alanine in 5-HT_{1A} had little effect on the potency of 4-F,5-MeO-tryptamines, but decreased the potency of serotonin and 4-F,5-OH-DMT by about 133-fold and 19-fold, respectively. As we only observed minor effects on DMT, we propose that N343$^{6.55}$ of 5-HT_{2A} forms a hydrogen bond with the 5-hydroxyl group during activation. We further suggest that the decreased 5-HT_{2A} potency of 4-fluorinated tryptamines is due to an already reduced ability of 5-MeO-DMT to form hydrogen bonds with N343$^{6.55}$, as addition of a fluorine further changes the electronic character of the 5-position oxygen.

Structures of therapeutic-bound 5-HT_{1A}

Although psychedelics are useful tools to study 5-HT receptor structure and function, a renewed interest in their actions has been sparked by their therapeutic potential in the treatment of psychiatric disorders, such as treatment-resistant depression and anxiety disorders[1,33]. Even though the contribution of 5-HT_{1A} activity to the clinical efficacy of tryptamines and ergolines remains unclear, 5-HT_{1A} is a bona fide therapeutic target for the clinically used anxiolytic buspirone and the antidepressant vilazodone. To better understand the molecular pharmacology of 5-MeO-DMT in the context of prescribed medications, we performed structural and functional characterizations of buspirone and vilazodone and compared them to that of 4-F,5-MeO-PyrT, a 5-HT_{1A}-selective analogue of the psychedelic 5-MeO-DMT (Fig. 4). As it is unknown how buspirone and vilazodone bind to 5-HT_{1A}, we determined cryo-EM structures of drug-bound 5-HT_{1A}–G_i complexes at nominal resolutions of 2.62 Å and 2.94 Å, respectively (Fig. 4, Extended Data Fig. 5 and Extended Data

Table 1). The binding pockets of all 5-HT_{1A}–drug complexes analysed here showed only subtle differences, with essentially all relevant side chains assuming similar states, except for an observed rotamer switch in the buspirone-bound receptor (described below). The indole core of vilazodone is bound to the OBP, forming a similar hydrogen bond with $T121^{3.37}$ as observed for 5-MeO-DMT and 4-F,5-MeO-PyrT. However, its benzofuran carboxamide group extends towards the extracellular site. Although this overall binding pose is reminiscent of aripiprazole (Abilify)[22], an antipsychotic and antidepressant, the piperazine moiety of vilazodone is located farther towards the extracellular space than observed in any of the other compounds (Fig. 4). This feature is probably due to the differing binding configurations of vilazodone and aripiprazole. Specifically, the N-aryl substituent of aripiprazole and the N-alkyl substituent of vilazodone bind to the OBP, and $D116^{3.32}$ and $Y390^{7.43}$ therefore interact with the same piperazine amine in both compounds. By contrast, buspirone assumes an unusual overall binding mode, whereby its azaspirodecane-7,9-dione group does not extend towards the extracellular space, as observed for the piperazine substituents of aripiprazole or vilazodone. Instead, buspirone adopts a kinked conformation in which the azaspirodecane-7,9-dione group bends into a crevice between TM2 and TM3. There it seems to displace the side chain of $F112^{3.28}$, which switches its rotamer conformation to face the membrane (Extended Data Fig. 5d). In the OBP, the piperazine of buspirone interacts with $D116^{3.32}$ in a similar fashion as observed for aripiprazole, and its pyrimidine group is located near TM3 and TM5, forming mostly hydrophobic interactions. Overall, we note that despite their diverse scaffolds, vilazodone, aripiprazole and buspirone assume similar poses in the core OBP, with their aromatic piperazine substituents primarily being stabilized by phenylalanines in TM6 ($F361^{6.51}$ and $F362^{6.52}$). 5-MeO-DMT and the 5-HT_{1A}-selective analogue 4-F,5-MeO-PyrT therefore exhibit similar binding modes as antidepressant medications in the OBP, which implies that these compounds have related pharmacological activities.

To test this hypothesis, we performed signalling assays to characterize and contrast the in vitro pharmacological activities of the different prescription drugs to those of 4-F,5-MeO-PyrT (Fig. 4). In BRET assays determining 5-HT_{1A}-mediated activation of G_{i1}, buspirone (maximum drug effect (E_{max}) = 93.4% of 5-HT), vilazodone (E_{max} = 97.4%) and 4-F,5-MeO-PyrT (E_{max} = 102.8%) were all high-efficacy agonists, whereas aripiprazole (E_{max} = 77.1%) showed modestly reduced efficacy. Note that vilazodone showed activity at concentrations as low as 30 pM, which we suspect is due to the slow binding kinetics of this drug. Vilazodone (G_i BRET EC_{50} = 480 pM) showed the highest potency of the medications tested, which could be partially due to its atypical binding mode. In addition to its similar binding mode in the OBP to that of prescribed antidepressants, the 5-HT_{1A}-selective indoleamine 4-F,5-MeO-PyrT (G_i BRET EC_{50} = 370 pM) showed comparable potency and efficacy to vilazodone. Although these findings underscore that 4-F,5-MeO-PyrT exhibits 5-HT_{1A} activity comparable to that of antidepressant medications, it also revealed subtle differences in their efficacies. This result is in line with our observation that vilazodone, buspirone and aripiprazole also bind to extended binding pockets (EBPs) and probably stabilize conformational ensembles distinct from that of 5-MeO-DMT and 4-F,5-MeO-PyrT. Thus, 4-F,5-MeO-PyrT as a 5-HT_{1A}-selective tryptamine could enable the exploration of 5-HT_{1A}-mediated behavioural aspects of 5-MeO-tryptamines.

In vivo activity of a 5-MeO-DMT derivative

We next tested the utility of 4-F,5-MeO-PyrT as a target-selective in vivo probe to interrogate the role of 5-HT_{1A} in both the hallucinogenic and the potential therapeutic effects of 5-MeO-tryptamines. Results from in vitro studies showed that 4-F,5-MeO-PyrT is more than 800-fold selective for 5-HT_{1A} over 5-HT_{2A} (Extended Data Fig. 6a and Supplementary Table 1). Moreover, the compound had substantially reduced activity at all other G protein-coupled 5-HT receptors, the serotonin transporter and other neurotransmitter transporters (Extended Data Fig. 6b,c). In mice, 4-F,5-MeO-PyrT brain penetration peaked 30 min following drug administration (total brain-to-plasma ratio of 3.3, unbound brain-to-plasma ratio of 0.91; peak plasma concentration ($C_{max/brain}$) = 143 ng ml^{-1} after 1 mg kg^{-1} subcutaneous (s.c.) administration), and the compound was largely cleared within 2 h (Fig. 5a and Extended Data Table 2). At 82.5% brain tissue binding, the estimated free drug concentration in the brain at the time for the peak plasma concentration (T_{max}) was about 100 nM following a s.c. dose of 1 mg kg^{-1}, which is anticipated to exert high 5-HT_{1A} engagement in vivo (G_i BRET EC_{50} = 370 pM), with substantially reduced engagement of 5-HT_{2A} (G_q BRET EC_{50} = 300 nM) (Extended Data Table 2 and Supplementary Table 1). To test these estimates in vivo, we examined in mice acute locomotor activity suppression (sedation) as a measure of 5-HT_{1A} activation and the head-twitch response (HTR) as a measure of 5-HT_{2A} activation[34]. We observed dose-dependent locomotor suppression in the open-field test for both 4-F,5-MeO-PyrT and 5-MeO-MET (Extended Data Fig. 7), a non-scheduled, balanced 5-HT_{1A} and 5-HT_{2A} agonist with near-identical in vitro activity to 5-MeO-DMT (Extended Data Fig. 6a). In HTR tests, 5-MeO-MET showed strong dose-dependent activity following co-administration of the 5-HT_{1A}-selective antagonist WAY-100635. This result indicated that HTR was suppressed by 5-HT_{1A} activation in our experimental design, which is a well-documented effect of 5-HT_{1A} agonism[35,36] (Fig. 5b). By contrast, 4-F,5-MeO-PyrT did not produce notable HTR at doses up to 3 mg kg^{-1} in the presence or absence of WAY-100635 (Fig. 5b and Extended Data Fig. 7d). 4-F,5-MeO-PyrT therefore does not display apparent 5-HT_{2A} activity in vivo following comparatively high doses (up to 100-fold higher than the lowest dose that produced suppression of locomotion: 0.03 mg kg^{-1}). Together, these data suggest that in vivo, 4-F,5-MeO-PyrT is highly potent and selective for 5-HT_{1A}, readily enters the brain and does not functionally engage 5-HT_{2A} at the tested doses.

As 5-MeO-DMT is reported to have anxiolytic and antidepressant activity in humans[10,37], we next investigated 5-HT_{1A}-mediated behaviours in preclinical models using 4-F,5-MeO-PyrT. We used a chronic social defeat (SD) stress model to induce a depressive-like phenotype in mice, which has been amply validated using selective serotonin reuptake inhibitors (chronic dosing) and ketamine (single administration)[38–40].

Male C57BL/6J mice were introduced to an unknown CD-1 aggressor mouse for 10 consecutive days of 10-min defeat bouts. Twenty-four hours after the last defeat bout, mice were tested in a two-part social interaction (SI) test (Fig. 5c). In the first phase, experimental mice were permitted to explore an open field (no target). In the second phase, a new unknown CD-1 aggressor mouse was placed into the enclosure (target). The interaction ratio (IR) was then determined by calculating the time that the experimental mouse spent in the

interaction zone during the no-target and target phases. Given the social nature of rodents, control mice tend to spend more time with the new target mouse than with the empty enclosure, whereas stress-susceptible mice exhibit a generalized avoidance of conspecifics and spend less time interacting with the new mouse[41,42].

To test the effect of 4-F,5-MeO-PyrT in this experiment, we injected 1 mg kg^{-1} of drug or vehicle (s.c.) 1 h after the last SD session on day 10, followed by the SI test 24 h after drug administration on day 11. This delayed readout reduced the confounding acute sedative effects of 4-F,5-MeO-PyrT and acts as a test of lasting therapeutic-like effects beyond initial drug exposure.

Results from the group that received vehicle confirmed that the SD paradigm induced social avoidance, as indicated by decreased IR values (Fig. 5d). This phenotype was rescued by 4-F,5-MeO-PyrT treatment, as indicated by an increased IR in the stress-exposed mice. Control mice that received either vehicle or drug did not show any distinguishable differences in IR, which indicated that the drug has measurable effects in a stress-experienced population. Results from mice co-administered with the selective 5-HT_{1A} antagonist WAY-100635 provided validation that the effects of 4-F,5-MeO-PyrT in this paradigm were indeed mediated by 5-HT_{1A}. WAY-100635 co-administration blocked the ability of 4-F,5-MeO-PyrT to ameliorate SI deficits in this model. Given the high affinity and selectivity of 4-F,5-MeO-PyrT and the inhibition of its behavioural effect by the established 5-HT_{1A} antagonist WAY-100635, these results suggest that the observed effects of 4-F,5-MeO-PyrT are mediated by 5-HT_{1A}.

We also recorded locomotor activity in a group of animals following SD and treatment with vehicle or 4-F,5-MeO-PyrT to eliminate the possibility of confounding factors due to decreased locomotion (Extended Data Fig. 7e). The amount of time each animal spent in the corners of the arena was also quantified. Vehicle-treated defeated mice spent more time in the corners, a result that confirmed previous observations that defeated mice not only show reduced SI but also engage in more vigilant, antisocial behaviours (Extended Data Fig. 7f,g). As expected, owing to the increased SI, this behaviour was no longer observed in drug-treated mice. It has been reported[42] that approximately one third of mice seem to be stress-resilient in this paradigm, as defined by a SI ratio of greater than 1. This effect potentially leads to an underestimation of the effect of 4-F,5-MeO-PyrT in our experiments. To account for this resilience and to determine whether 4-F,5-MeO-PyrT treatment could increase the proportion of resilient mice, we compared vehicle-treated and drug-treated stressed animals. The results showed that 4-F,5-MeO-PyrT increased the number of resilient mice (Extended Data Fig. 7h). Together, these findings further support the conclusion that 4-F,5-MeO-PyrT treatment ameliorates stress-related social deficits.

To evaluate additional depressive-like behaviours induced by SD, we investigated anhedonia using a sucrose-preference test immediately following SI[42] (Fig. 5e). Mice were allowed ad libitum access to two bottles: one containing water and the other 1% sucrose. Stressed mice treated with vehicle had a significantly reduced preference for sucrose compared with non-stressed mice, results that validate the depressive-like phenotype induced by SD. By contrast, stressed mice treated with 4-F,5-MeO-PyrT had significantly increased sucrose

preference relative to vehicle-treated animals and were essentially indistinguishable from non-stressed mice treated with vehicle or drug. As observed for the SI experiment, co-administration of WAY-100635 reversed the effects of 4-F,5-MeO-PyrT in stressed animals, which suggests that the anti-anhedonic effect of 4-F,5-MeO-PyrT is mediated by 5-HT_{1A}. WAY-100635 treatment alone seemed to increase sucrose preference in stressed mice; however, this effect was not significant, and a similar effect was not observed in the SI experiment.

Together, these data demonstrate that 4-F,5-MeO-PyrT can ameliorate social deficits and anhedonia in a SD mouse model in a similar fashion as has been shown for ketamine and selective serotonin reuptake inhibitors[38,43,44]. Therefore, 5-HT_{1A} might play a key part in the observed therapeutic effects of 5-MeO-tryptamines.

Discussion

Recent preliminary clinical data suggest that 5-MeO-DMT is a promising transdiagnostic therapeutic with rapid and lasting effects. Our work and previous studies have shown that 5-MeO-DMT has comparable signalling potency and efficacy at 5-HT_{1A} and 5-HT_{2A} in vitro, and both receptors contribute to its in vivo pharmacology[5,21,34]. In light of previous work showcasing 5-HT_{2A}-selective agonists that alleviate anxiety-like and depression-like states in preclinical models[15,16], we wanted to investigate the role of 5-HT_{1A} in both psychedelic and therapeutic effects of 5-MeO-tryptamines. Although 5-HT_{1A} is a validated therapeutic target for several approved medications, including vilazodone[12] and buspirone[8], the importance of 5-HT_{1A} agonism to the therapeutic effects of tryptamine psychedelics has not been conclusively addressed.

Because 5-HT_{2A} is responsible for the visual and other sensory disturbances elicited by classical psychedelics, it is typically assumed that these receptors also mediate therapeutic effects. There is currently no clinical evidence to support this hypothesis, and the pre-clinical evidence is mixed. The 5-HT_{2A} antagonist ketanserin did not block psilocybin-mediated attenuation of anhedonia induced by chronic stress in mice[45], whereas in another study, ketanserin blocked 5-MeO-DMT-mediated effects in a forced-swim test[4]. In the latter study, psilocybin-mediated attenuation of anhedonia was abolished in 5-HT_{2A} knockout mice[4]. Similarly, synaptogenesis readouts considered relevant for the therapeutic effects of psychedelics were not mediated by 5-HT_{2A} in one study, whereas synaptic remodelling was 5-HT_{2A}-dependent in another study[46,47].

Our finding that 4-F,5-MeO-PyrT, a highly 5-HT_{1A}-selective agonist, rescued SI deficits and anhedonia in mice induced by a SD model is therefore of considerable interest and has potential implications for the therapeutic effects of 5-MeO-tryptamines. These data also support the proposed complementary contributions of 5-HT_{1A} and 5-HT_{2A} to stress-coping mechanisms on a psychological[17] and a cellular level[48], the role of 5-HT_{1A} in stress resilience[49], as well as the reported antidepressant efficacy of clinical[12] and preclinical[50] 5-HT_{1A} drugs. Furthermore, our results show that 5-HT_{1A}-selective tryptamines lack the preclinical indications of classical psychedelic effects (for example, HTR), which suggests that some of these compounds may not be hallucinogenic while retaining therapeutic effects.

With respect to acute psychedelic effects, studies suggest that receptors other than 5-HT_{2A} also modulate subjective experience. LSD has recently been reported to enhance emotional empathy and prosocial behaviour in healthy volunteers; however, the empathogenic effect was not blocked by ketanserin[51]. Other studies specifically point to a major role of 5-HT_{1A}, as the 5-HT_{1A} antagonist pindolol increased the subjective psychedelic effects of DMT[52]. Moreover, the 5-HT_{1A} agonist buspirone attenuates the visual hallucinogenic effects of psilocybin in healthy volunteers[53], which implies that the distinct subjective effects of the psychedelic experience of 5-MeO-DMT could be shaped by 5-HT_{1A}. Examination of the anecdotal reports on 5-MeO-DMT analogues studied herein reveals a myriad of psychoactive effects[28] (Supplementary Table 2). However, systematic human data are not available to enable meaningful correlation between the subjective experience of different 5-MeO-DMT derivatives and 5-HT_{1A} potency, and/or relative potency of 5-HT_{1A} and 5-HT_{2A}. It should be noted though that 5-MeO-PyrT, an analogue for which we report >38-fold selectivity for 5-HT_{1A} over 5-HT_{2A}, induces effects described as white-out and amnesia[28] (Supplementary Table 2). Although 5-MeO-DMT has some amnesic elements to its subjective experience[54], this effect seems to be amplified in 5-MeO-PyrT[28], which indicates that 5-HT_{1A} activation by 5-MeO-tryptamines has a possible role in the mediation of these brain states and effects.

Despite the importance of 5-HT_{1A} in the effects of psychedelics, comparatively little is known about the structural pharmacology of different psychedelics at 5-HT_{1A}. We addressed this important gap in knowledge in the current work by integrating cryo-EM with systematic receptor mutagenesis and medicinal chemistry. Together, we provide both a global comparative map of receptor structural pharmacology for different drug classes and detailed analyses of crucial binding areas and specific amino acid residues that determine the signalling potency and efficacy at 5-HT_{1A}, as well as the selectivity for 5-HT_{1A} over 5-HT_{2A}. We uncovered how receptor-specific subpockets determine both the potency and efficacy of tryptamine ligands at both receptors. Our findings provide a structure-guided framework that enables the development of tryptamine probes with finely tuned pharmacological activities and varying degrees of 5-HT_{1A} and 5-HT_{2A} selectivity, including potent and highly 5-HT_{1A}-selective compounds. Moreover, we elucidated how 5-MeO-DMT and a selective analogue engage 5-HT_{1A} in an almost identical way, thereby showcasing the usefulness of this probe in studying 5-HT_{1A}-mediated aspects of 5-MeO-DMT. These binding poses partially overlap with those of the 5-HT_{1A}-targeting medications buspirone, vilazodone and aripiprazole[22]. However, these medications occupy EBPs, which indicate the stabilization of distinct conformational ensembles and therefore the generation of signal outputs distinct from those of psychoactive tryptamines. These differences, as well as their engagement of other targets[7,55], probably have a role in the different physiological effects of these medications compared with the psychedelic 5-MeO-DMT, but further experiments are required to investigate the precise correlates in detail. Nonetheless, we demonstrated that modification of the 5-MeO-DMT scaffold can produce highly selective probes that engage 5-HT_{1A} in a structural and pharmacological manner that is similar to clinical drugs. Of note, the anxiolytic-like and antidepressant-like effects of these probes emphasize their utility in elucidating 5-HT_{1A}-mediated effects of tryptamine psychedelics in vivo and potentially facilitate the exploration of therapeutic applications in future work.

Online content

Any methods, additional references, Nature Portfolio reporting summaries, source data, extended data, supplementary information, acknowledgements, peer review information; details of author contributions and competing interests; and statements of data and code availability are available at https://doi.org/10.1038/s41586-024-07403-2.

Methods

Chemical synthesis

Compounds were synthesized as depicted in Supplementary Data 1. Compounds not synthesized in-house were purchased from the following sources: 5-HT (Sigma), 5-MeO-DMT (Cayman Chemicals), DMT (Cayman Chemicals), psilocin (Cayman Chemicals), 4-OH-MET (Cayman Chemical), LSD (Cayman Chemicals), mescaline (Cayman Chemicals), vilazodone (Sigma), buspirone (Alfa Aesar), bufotenine (Cayman Chemical), aripiprazole (Sigma), citalopram (TCI), FFN246 (Aobious), IDT307 (Sigma), ASP+ (Invitrogen), WAY-100635 (Biovision), 8-OH-DPAT (MedChemExpress), SEP-363856 (MedChemExpress), *N*-(1-napthyl)piperazine (Alfa Aesar), tandospirone (Toronto Research Chemicals) and gepirone (Toronto Research Chemicals).

Most tryptamines were synthesized from commercially available indoles (unless otherwise specified) in a sequence of oxalylation, glyoxy esterification, reduction, bromination and finally *N*-alkylation. In other cases, the Speeter–Anthony route was applied[30]. 7-Azaindole tryptamines were obtained through acylation with bromoacetylbromide, followed by reduction and *N*-alkylation. For the purification of the compounds, preparative TLC (1,000 micron plates) or silica gel chromatography for large-scale reactions was used. Compound characterization, including confirmation of the chemical identity and purity, was accomplished by ^{1}H, ^{13}C and ^{19}F nuclear magnetic resonance and high-resolution mass spectrometry. For detailed synthetic procedures and analytical data, see Supplementary Information.

Constructs and expression

Structural studies reported herein were performed with a 5-HT_{1A} construct based on previous work[22]. In brief, human 5-HT_{1A} (UniProtKB identifier P08908) was cloned into a modified pFastBac vector and a cleavable HA-signal sequence followed by a Flag tag, a 10×His tag and a TEV protease site was introduced at the amino terminus. In addition, the first 24 residues were replaced with BRIL, and a L125W$^{3.41}$ mutation was introduced to increase expression levels. Heterotrimeric G protein was expressed from a single multibac virus following previous construct design[13]. In brief, N-terminally 6×His-tagged human $G\beta_1$ was cloned under the control of a polyhedrin promoter, whereas a $G\gamma_2$–$G\alpha_{i1}$ fusion construct was cloned under the control of a P10 promoter. $G\gamma_2$ and $G\alpha_{i1}$ were fused with a GSAGSAGSA linker. The 5-MeO-DMT–5-HT_{1A}–$G\alpha_{i1}$–$G\beta_1$–$G\gamma_2$ and buspirone–5-HT_{1A}–$G\alpha_{i1}$–$G\beta_1$–$G\gamma_2$ structures used a $G\alpha_{i1}$ protein containing four individual point mutations (S47N, G203A, E245A and A326S) to enhance the stability of the heterotrimeric G protein (dominant-negative)[22]. Protein expression was done in Sf9 cells (Expression Systems) using

the Bac-to-Bac Baculovirus expression system (Invitrogen), for which bacmid DNA was generated in DH10Bac cells (Invitrogen). Initial P0 virus was obtained through the addition of about 3 μg recombinant bacmid DNA with 3 μl FuGENE HD transfection reagent (Promega) in 100 μl Sf900 II medium (Invitrogen) to 500,000 Sf9 cells plated in 2 ml of SF900 II medium in wells of a 12-well plate. After 5 days at 27 °C, the supernatant was collected as viral stock, and high-titre recombinant P1 baculovirus (>10^9 virus particles per ml) was generated by adding 300 μl P0 to 30 ml of 3 × 10^6 cells per ml and incubating cells at 27 °C for 3 days. Approximate titres were estimated by flow cytometry analysis staining P1-infected cells with gp64-PE antibody (Expression Systems). Expression of both 5-HT_{1A} and heterotrimers was done separately by infecting Sf9 cells at a cell density of 2–3 × 10^6 cells per ml with P1 virus at a multiplicity of infection of 5. After 48 h of shaking at 27 °C, cells expressing either receptor or G-protein were collected by centrifugation (2,500*g*, 15 min, 4 °C) at 48 h after infection and stored at −80 °C until use.

5-HT_{1A} purification

For 5-HT_{1A} purification, insect cell membranes were disrupted by thawing frozen cell pellets in a hypotonic buffer containing 10 mM HEPES pH 7.5, 10 mM $MgCl_2$, 20 mM KCl and home-made protease inhibitor cocktail (500 μM AEBSF, 1 μM E-64, 1 μM leupeptin and 150 nM aprotinin) (Gold Biotechnology). Total cellular membranes were spun down and washed twice by homogenization in a manual dounce homogenizer using around 30 strokes followed by centrifugation (125,000*g*, 40 min, 4 °C) in a high osmotic buffer containing 1 M NaCl, 10 mM HEPES pH 7.5, 10 mM $MgCl_2$, 20 mM KCl and home-made protease inhibitor cocktail. Purified membranes were directly flash-frozen in liquid nitrogen and stored at −80 °C until further use.

For the formation of 5-HT_{1A}–drug complexes, membranes were suspended in buffer containing 10 mM HEPES pH 7.5, 10 mM $MgCl_2$, 20 mM KCl, 150 mM NaCl, home-made protease inhibitor cocktail and 20 μM 5-MeO-DMT (Cayman Chemicals), LSD (Cayman Chemicals), 4-F,5-MeO-PyrT (synthesized in-house), vilazodone (Sigma) or buspirone (Alfa Aesar). Drug complexation was initiated through agitation for 1 h at room temperature followed by equilibration at 4 °C, addition of 2 mg ml^{-1} final concentration of iodoacetamide (Acros Organics) and subsequent solubilization through the addition of a final concentration of 1% (w/v) *n*-dodecyl-β-D-maltopyranoside (DDM; Anatrace), 0.2% (w/v) cholesteryl hemisuccinate (CHS; Anatrace) and home-made protease inhibitor cocktail for 2 h at 4 °C. Unsolubilized material was then removed by centrifugation (200,000*g*, 30 min, 4 °C), and imidazole was added to the supernatant to a final concentration of 20 mM. Proteins were bound to TALON IMAC resin (Clontech). Protein-bound TALON resin was washed with 10 column volumes (c.v.) of wash buffer I (50 mM HEPES, pH 7.5, 800 mM NaCl, 0.1% (w/v) DDM, 0.02% (w/v) CHS, 20 mM imidazole, 10% (v/v) glycerol and 10 μM drug). The detergent was then exchanged for lauryl maltose neopentyl glycol (LMNG) by incubating the protein-bound TALON with wash buffer I supplemented with 0.1% LMNG for 1 h at 4 °C followed by successive washes with the following buffers: wash buffer II (50 mM HEPES, pH 7.5, 800 mM NaCl, 0.05% (w/v) LMNG and 0.01% (w/v) CHS), wash buffer III (50 mM HEPES, pH 7.5, 800 mM NaCl, 0.01% (w/v) LMNG and 0.002% (w/v) CHS) and wash buffer IV (25 mM HEPES, pH 7.5, 500 mM NaCl,

0.005% (w/v) LMNG and 0.001% (w/v) CHS). After the final incubation step, the proteins were eluted with 25 mM HEPES, pH 7.5, 500 mM NaCl, 0.005% (w/v) LMNG, 0.001% (w/v) CHS, 10 μM drug and 250 mM imidazole. The eluted proteins were concentrated using Vivaspin 6 centrifugal concentrators (Sartorius), and imidazole was removed from the protein solution by applying the sample to a PD MiniTrap sample column (Cytiva) according to the manufacturer's protocol. The resulting protein sample was incubated with 200 μg of TEV protease overnight. The following day, the protein mixture was incubated with TALON resin for 10 min at 4 °C to remove TEV and uncleaved protein from the solution. The cleaved protein samples were further concentrated and immediately used for complexation. General protein purity and monodispersity was assessed by SDS–PAGE and analytical size-exclusion chromatography.

G protein purification

For G protein purification, Sf9 insect cells were homogenized in the following lysis buffer: 20 mm HEPES, pH 7.5, 100 mM NaCl, 1 mM $MgCl_2$, 0.01 mM guanosine diphosphate, 10% glycerol, 5 mM β-mercaptoethanol, 30 mM imidazole, 0.2% Triton X-100 and home-made protease inhibitor cocktail (500 μM AEBSF, 1 μM E-64, 1 μM leupeptin and 150 nM aprotinin). The cytoplasmic and membrane fractions were separated by centrifugation (50,000*g*, 20 min, 4 °C). The resulting supernatant was subjected to an additional centrifugation step (200,000*g*, 45 min, 4 °C) to remove insoluble material and protein aggregate. The final supernatant was bound to HisPur Ni-NTA resin (Thermo Scientific) overnight at 4 °C. Protein-bound Ni-NTA resin was washed with 20 c.v. lysis buffer lacking 0.2% Triton X-100 followed by 20 c.v. lysis buffer lacking 0.2% Triton X-100 and 30 mM imidazole. Protein was eluted from the resin with lysis buffer lacking Triton X-100 and supplemented with 300 mM imidazole. The eluent was concentrated using Vivaspin 6 centrifugal concentrators (Sartorius). Imidazole was removed from the concentrated eluent using PD MiniTrap sample preparation columns (Cytiva) according to the manufacturer's protocol. Eluted protein was further processed through the addition of PreScission Protease (Genscript) to remove the N-terminal His tag from the $G\beta_1$ subunit. Purified G protein and PreScission Protease were incubated overnight at 4 °C to facilitate cleavage. Cleaved G proteins were separated from PreScission Protease and uncleaved proteins by 15 min incubation with TALON resin at 4 °C. Cleaved G proteins were concentrated for immediate use or flash frozen and stored at −80 °C.

Formation of receptor–G protein complexes, purification and grid preparation

To assemble drug-bound 5-HT_{1A}–G_i complexes, we mixed purified receptor (500–1,000 μg at a molecular weight of approximately 55.4 kDa) with purified heterotrimer (1,000–2,000 μg at a molecular weight of approximately 86.4 kDa) at a molar ratio of 1:1.2 in a total volume of 110 μl. The final buffer was adjusted to 20 mM HEPES, pH 7.5, 120 mM NaCl, 5 mM $CaCl_2$, 2.5 mM $MgCl_2$, 0.001% (w/v) LMNG, 0.0002% (w/v) CHS and 10 μl drug, and supplemented with 25 mU per ml apyrase before incubation overnight at 4 °C. The next day, samples were concentrated and finally purified over a S200 size-exclusion chromatography column equilibrated in 20 mM HEPES, pH 7.5, 100 mM NaCl, 0.001%(w/v) LMNG, 0.0002% (w/v) CHS, 0.00025% GDN and 1–10 μM drug. Peak fractions were then pooled, concentrated to about 15–30 mg ml^{-1} and immediately used to prepare grids for cryo-EM

data collection. To prepare cryo-EM grids for imaging, 3 μl of the samples was applied to glow-discharged holey carbon EM grids (Quantifoil 300 copper mesh, R1.2/1.3) in an EM-GP2 plunge freezer (Leica). An EM-GP2 chamber was set to 95% humidity at 12 °C. Sample-coated grids were blotted for 3–3.3 s before plunge-freezing into liquid ethane and stored in liquid nitrogen for data collection.

Cryo-EM data collection and processing

All automatic data collection was performed on FEI Titan Krios instruments equipped with Gatan K3 direct electron detectors either operated by the Simons Electron Microscopy Center in the New York Structural Biology Center or the Laboratory of BioMolecular Structure at Brookhaven National Laboratory. The microscopes were operated at 300 kV accelerating voltage, at a nominal magnification of 64,000–81,000 corresponding to pixel sizes of 0.41–0.538 Å. For each dataset, at least 3,500 movies were obtained at a dose rate of 25–30 electrons per $Å^2$ per s with a defocus ranging from −0.5 to −1.8 μm. The total exposure time was 2 s and intermediate frames were recorded in 0.05 s intervals, resulting in an accumulated dose of 50–60 electrons per $Å^2$ and a total of 40 frames per micrograph.

Movies were motion-corrected using MotionCor2 (ref. 56) and imported to cryoSPARC[57] for further processing. Contrast transfer functions were estimated using patchCTF in cryoSPARC. An initial model was produced from a subset of micrographs using blob picking, followed by extraction, 2D classification, selection of key classes and generation of a model ab initio. Subsequent map models were produced from a curated micrograph set using particles found by picking using the initial map model as a template. Particles were extracted, subjected to 2D classification and a final particle stack was obtained by iterative rounds of 3D classification generating several bad models from rejected particles as a sink in hetero-refinement. A final map was obtained using NU-refinement[58]. Structures were built in Coot[59] based on a previous 5-HT_{1A}–G_i complex structure[22], and further refined using PHENIX[60] and ServalCat[61]. Sterols were built as cholesterol hemisuccinate; however, we cannot fully rule out the possibility that some of these densities stem from cholesterol co-purified with the receptor. Final maps were imported to PyMOL[62] and UCSF Chimera for generating figures shown in the manuscript.

5-HT_{1A}-mediated cAMP reduction assay

Reduction in cellular cAMP levels mediated by 5-HT_{1A} was determined in HEK293-T cells (American Type Culture Collection) using a cAMP biosensor (GloSensor, Promega)[25,32]. First, HEK293-T cells were cultured in Dulbecco’s modified Eagle medium (DMEM) supplemented with 10% (v/v) FBS and penicillin–streptomycin (Invitrogen). For transfection, cells were plated in 10 cm plates and medium was exchanged to DMEM supplemented with 1% (v/v) dialysed FBS (dFBS). Once cells reached 6–7 million in a 10 cm plate, transfection was done, forming particles in 500 μl Opti-MEM (Invitrogen) using 4 μg of human 5-HT_{1A} with a N-terminal HA signal sequence and Flag tag cloned into a pcDNA3 vector, 4 μg of GloSensor DNA and 16 μl of polyethyleneimine (PEI; Alfa Aesar). The following day, medium was aspirated, and cells were trypsinized and plated into each well of a poly-L-lysine-coated clear-bottom 384-well plate (Greiner Bio One) in DMEM supplemented with 1% (v/v) dFBS. Next, 40 μl of cells at a density of 500,000 per ml were

plated per well. The next day, medium was aspirated and D-luciferin (Gold Biotechnology) was loaded into cells by adding 30 µl of a 1.2 mM solution in Hank's balanced salt solution (HBSS) supplemented with 20 mM HEPES pH 7.4, 0.1% BSA (w/v) and 0.01% ascorbic acid (w/v). Loading was performed at 37 °C for 1 h, followed by addition of 15 µl of drug solutions at 3× concentration for 15 min at room temperature. To measure agonist activity for 5-HT_{1A}, we added 15 µl of isoproterenol in HBSS supplemented with 20 mM HEPES pH 7.4 at a final concentration of 400 nM (to activate Gs through endogenous adrenergic receptors). Luminescence intensity was determined 15 min later in a MicroBeta TriLux liquid scintillation counter (Perkin Elmer). Data were plotted and analysed using GraphPad Prism 8.0.

5-HT_{7A}-mediated cAMP stimulation assay

HEK293-T cells were cultured and transfected as described above with 4 µg of human 5-HT_{7A} with a N-terminal HA signal sequence and Flag tag cloned into a pcDNA3 vector and 4 µg of GloSensor DNA[25,32]. Transfected cells were split, plated and loaded with luciferin in the same manner as described above. Cells were stimulated with 15 µl of drug solutions at 3× concentration for 30 min at room temperature. Assay plates were read immediately after following incubation in a MicroBeta TriLux liquid scintillation counter (Perkin Elmer). Data were plotted and analysed using GraphPad Prism 8.0.

BRET signalling assays

We determined both 5-HT_{1A}-mediated activation of heterotrimeric G_{i1} ($G\alpha_{i1}$–$G\beta_3$–$G\gamma_9$) and 5-HT_{2A}-mediated activation of heterotrimeric G_q (G_q–$G\beta_3$–$G\gamma_9$) using previously published TRUPATH reporter constructs[18]. Assays were essentially performed as previously described. In brief, receptor as well as RLuc-Gα, Gβ and eGFP–Gγ constructs were transfected with PEI (Alfa Aesar) into HEK293-T cells using a ratio of 1:1:1:1 (5-HT_{1A}:$G\alpha_{i1}$:$G\beta_3$:$G\gamma_9$) and 2:5:5:5 (5-HT_{2A}:G_q:$G\beta_3$:$G\gamma$9). Typically, we transfected 6–7 million cells in DMEM supplemented with 1% (v/v) dFBS in a 10 cm plate with a total of 8 µg of DNA. The next day, 20,000 cells were plated into each well of a poly-L-lysine-coated white-bottom 384-well plate (Greiner Bio One) in DMEM supplemented with 1% (v/v) dFBS. The following day, the day of the experiment, medium was aspirated and the cells were washed with HBSS supplemented with 20 mM HEPES pH 7.4. Next, 15 µl of drug solutions at 3× concentration were added in 30 µl HBSS supplemented with 20 mM HEPES pH 7.4, 0.1% (w/v) BSA and 0.01% (w/v) ascorbic acid. Cells were incubated for 30 min at 37 °C followed by addition of 15 µl of freshly prepared 30 µM coelenterazine 400a (Gold Biotechnology). Plates were then immediately read in a Victor NIVO plate reader (Perkin Elmer) with 395 nm (RLuc8-coelenterazine 400a) and 510 nm (GFP2) emission filters, at integration times of 1 s per well. BRET2 ratios were computed as the ratio of the GFP2 emission to RLuc8 emission. Data were plotted as a function of drug concentration, normalized to the per cent of 5-HT stimulation, and analysed using 'log(agonist) vs. response' in GraphPad Prism 8.0.

Arrestin recruitment assay

To determine off-target effects, we performed PRESTO-Tango β-arrestin2 recruitment assays for all 5-HT receptors essentially as previously described[63]. The receptor constructs

were obtained from Addgene and contain the TEV cleavage site and the tetracycline transactivator (tTA) fused to the C terminus of the receptor. For the assay, constructs were transfected into HTLA cells (provided by B. Roth, University of North Carolina), which express TEV-fused β-arrestin2 and a tTA-driven luciferase and are necessary for this assay. A day before the assay, cells were cultured in DMEM supplemented with 1% dFBS and transfected with 8 μg of DNA per 7 million cells in a 10 cm plate using PEI-mediated transfection. The next day, 20,000 cells in 40 μl were then plated in poly-L-lysine-coated clear-bottom 384-well plates in the same medium and incubated for at least 5 h before stimulation. Next, 20 μl drug solutions in HBSS supplemented with 20 mM HEPES pH 7.4, 0.1% (w/v) BSA and 0.01% (w/v) ascorbic were then added for overnight incubation. After 16–24 h of overnight incubation, medium and drug solutions were aspirated and 20 μl per well of BrightGlo reagent (purchased from Promega, after 1:20 dilution) was added per well. The plate was incubated for 20 min at room temperature in the dark before being counted using a MicroBeta TriLux liquid scintillation counter. Relative luminescence units were then plotted as a function of drug concentration and compared to 5-HT stimulation.

Neurotransmitter transport assays

Serotonin transporter uptake inhibition.—For determining inhibition of serotonin transporter (SERT) uptake, HEK293-T cells were cultured in DMEM supplemented with 10% (v/v) FBS and penicillin–streptomycin (Invitrogen). For transfection, cells were plated in 10 cm plates and medium was exchanged to DMEM supplemented with 1% (v/v) dFBS. Once cells reached 6–7 million in a 10 cm plate, a transfection mixture composed of 8 μg of SERT cloned into a pcDNA3 vector, 500 μl of OptiMEM and 16 μl of PEI was added dropwise to the cells. The following day, transfected cells were trypsinized and plated at a density of 25,000 cells per well of a poly-L-lysine coated clear-bottom 384-well plate. The uptake inhibition assay was performed the following day. Medium was aspirated and cells were washed with HBSS supplemented with 20 mM HEPES pH 7.4. To each well, 30 μl of HBSS containing 20 mM HEPES, 0.1% BSA and 0.01% ascorbic acid and 15 μl of drug dilutions at 3× concentrations were added. Cells were then incubated at 37 °C for 45 min. A final concentration of 10 μM FFN246 (Aobious)[64] was added to each well, and cells were incubated for an additional 1 h at 37 °C. The contents of each well were then aspirated, and each well was washed twice with HBSS supplemented with 20 mM HEPES pH 7.4. Next, 50 μl of HBSS supplemented with 20 mM HEPES pH 7.4 was added to each well, and the assay plate was read using a Victor NIVO plate reader using 355 nm excitation and 435 nm emission filters, and measuring over 0.1 s. Data were plotted as a function of drug concentration, normalized to the per cent of citalopram inhibition and analysed using ‘log(inhibitor) vs. response’ in GraphPad Prism 8.0.

OCT1, OCT2 and PMAT uptake inhibition.—Inducible cell lines stably expressing OCT1, OCT2 or PMAT were generated in-house using the Flp-In T-Rex cell line (ThermoFisher) according to the manufacturer’s recommendations. Cells were maintained in DMEM supplemented with 10% FBS, 100 μg ml^{-1} hygromycin B (Gold Biotechnology) and 10 μg ml^{-1} blasticidin (Gold Biotechnology). To measure uptake inhibition, cells were seeded into poly-L-lysine-coated clear-bottom 384-well plates at a density of 25,000 cells per well in DMEM containing 10% FBS and 2 μg ml^{-1} tetracycline (Sigma) to induce

transporter expression. At 24 h following induction, medium was aspirated and cells were washed with HBSS supplemented with 20 mM HEPES pH 7.4. To each well, 30 µl of HBSS with 20 mM HEPES pH 7.4, 0.1% (w/v) BSA and 0.01% ascorbic acid was added followed by 15 µl of drug dilutions at 3× concentration. Cells were incubated with drug for 30 min at 37 °C. Fluorescent substrate was then added to the cells. To measure inhibition of OCT1 and PMAT, a final concentration of 12.5 µM of IDT307 (Sigma) was used, whereas for OCT2, a final concentration of 5 µM of the fluorescent substrate ASP+ (ThermoFisher) and 250 µM trypan blue was added. Cells were incubated with respective substrates for 1 h at 37 °C. OCT2 cells were read directly in a Victor NIVO plate reader using 495 nm excitation and 580 emission filter for 0.1 s. OCT1 and PMAT cells were washed in HBSS supplemented with 20 mM HEPES pH 7.4 before reading in a Victor NIVO plate reader using 435 nm excitation and 480 nm emission filter for 0.1 s.

Cell lines

None of the cell lines used in this study were authenticated using independent methods. All cell lines were regularly tested for mycoplasma contamination.

Animal studies

The Icahn School of Medicine at Mount Sinai, Columbia University and Sai Life Sciences Limited are accredited by the Association for Assessment and Accreditation of Laboratory Animal Care International. All described experiments involving mice were approved by the Institutional Animal Care and Use Committee at the Icahn School of Medicine at Mount Sinai, Columbia University or Sai Life Sciences Limited to comply with ethical regulations. Male 8–15-week-old C57BL6/J mice were used as the experimental mice for all experiments. CD-1 retired breeders were used as aggressors and ranged from 4 to 6 months of age. Animals received regular veterinary care (weekly by institutional veterinarians), including daily health monitoring (by experimenters) of the animals (observing home cage behaviours, nesting and body weight). All procedures were designed to minimize any stress or distress. Mice were purchased from the Jackson Laboratory and housed 5 mice per cage with food and water available ad libitum. Mice were maintained on a 12-h light–dark cycle (lights on 7:00–19:00) and all testing was done in the light cycle. Temperature was kept constant at 22 ± 2 °C, and relative humidity was maintained at 50 ± 5%.

Drug preparation and administration for animal studies

All samples are prepared the same day testing was performed. Solids were weighed into small vials and dissolved in USP-grade 0.85% saline with the addition of 2 molar equivalents of glacial acetic acid. Sonication and gentle heating were applied until complete dissolution. The compounds were subsequently filtered through 0.45 µm filters into a new glass vial. All compounds were administered at a selected s.c. dose.

Pharmacokinetics studies

Studies were conducted at Sai Life Sciences Limited. A total of 27 healthy C57BL/6 male mice were used in this study with 3 mice per time point. Animals were administered s.c. with a solution formulation of the compound at the indicated dose. Blood samples

(approximately 60 µl) were collected under light isoflurane anaesthesia (Surgivet) from the retro-orbital plexus from a set of 3 mice at 0.083, 0.25, 0.5, 1, 2, 4, 8 and 12 h. Immediately after blood collection, plasma was collected by centrifugation at 4,000 r.p.m. for 10 min at 40 °C and samples were stored at −70 ± 10 °C until analyses. Following blood collection, animals were immediately euthanized and the abdominal vena cava was cut open. The whole body was then perfused from the heart using 10 ml of saline. Brain samples were collected from set of 3 mice at 0.083, 0.25, 0.5, 1, 2, 4, 8 and 12 h. After isolation, brain samples were rinsed 3 times in ice-cold saline for 5–10 s per rinse using 5–10 ml saline and subsequently dried on blotting paper. Brain samples were homogenized using ice-cold PBS (pH 7.4). Total homogenate volume was three times the tissue weight. All homogenates were stored below −70 ± 10 °C until analyses.

Concentrations of the compound in mouse plasma and brain samples were determined by LC–MS/MS. The non-compartmental-analysis tool of Phoenix WinNonlin (v.8.0) was used to assess the pharmacokinetics parameters. C_{max} and T_{max} were the observed values. The areas under the concentration time curve (AUC_{last}) was calculated using the linear trapezoidal rule. The terminal elimination rate constant, k_e, was determined by regression analysis of the linear terminal portion of the log plasma concentration–time curve. Tissue K_p values were calculated using Microsoft excel.

Plasma protein and brain tissue binding

Studies were conducted at Sai Life Sciences Limited. Previously frozen mouse plasma was thawed at room temperature. An aliquot of 1,000 µl was aliquoted into microcentrifuge tubes and incubated at 37 °C for 10 min. A volume of 5 µl of 4-F,5-MeO-PyrT or control drug from 1 mM DMSO stock was spiked into 995 µl of preincubated plasma to obtain 5 µM final concentration. Inserts were placed in a Teflon plate. Each insert was placed in the same orientation for easy recognition of the sample and buffer chamber. Next, 200 µl aliquots of 4-F,5-MeO-PyrT or control drug were added at 2 µM concentration ($n = 2$) in the red chamber and 350 µl of 50 mM PBS (pH 7.4) to the white chamber of the inserts. The red device was then sealed with an adhesive film and incubated at 37 °C with shaking at 100 r.p.m. for 4 h. For recovery and stability samples, 50 µl aliquots of 4-F,5-MeO-PyrT or control drug were added in 96-well deep-well plates and quenched with 400 µl acetonitrile (for 0 min). The remaining sample was incubated at 37 °C for 4 h. Following dialysis, 50 µl of aliquot was taken from each well (both red and white chamber) and diluted with equal volume of the opposite matrix to nullify the matrix effect. Similarly, 50 µl of PBS was added to recovery and stability samples. An aliquot of 100 µl was analysed by LC–MS/MS.

Open-field locomotion assay

Open-field locomotion evaluation was performed by trained observers who were blinded to both drug and dose. Male 10–15 week old C57BL/6J mice were allowed to habituate for 30 min. Mice were randomly administered with vehicle or WAY-100635 (1 mg kg^{-1} or 2 mg kg^{-1}, s.c.). Fifteen minutes after the pretreatment injection, mice were administered either 4-F,5-MeO-PyrT (0.1, 0.3, 1 or 3 mg kg^{-1}, s.c.) or 5-MeO-MET (0.3, 1, 3 or 10 mg kg^{-1}, s.c.) and immediately gently placed in a clear Plexiglass arena (27.31 × 27.31 × 20.32 cm, Med Associates ENV-510) lit with ambient light (about 330 lux) and allowed

to ambulate freely for 30 min. A separate cohort was gently placed in the Plexiglass arena immediately after receiving a subcutaneous injection of 4-F,5-MeO-PyrT (0.03, 0.1, 0.3, 1 or 3 mg kg^{-1}, s.c.) and allowed to ambulate freely for 120 min. The locomotion of the animals was tracked by infrared beams embedded along the *x, y* and *z* axes of the area and automatically recorded. Data were collected using Activity Monitor by Med Associates.

HTR assay

HTR evaluation was performed by trained observers who were blinded to both drug and dose. Male 10–15 week old C57BL/6J mice were habituated to the testing room for 30 min. The body weight of each mouse was recorded. HTR was defined as a rapid rotational movement of the head around the longitudinal axis of the animal's body. Mice were randomly administered with vehicle or WAY-100635 (1 mg kg^{-1} or 2 mg kg^{-1}, s.c.). Fifteen minutes after the pretreatment injection, mice were administered either 4-F,5-MeO-PyrT (0.1, 0.3, 1 or 3 mg kg^{-1}, s.c.) or 5-MeO-MET (0.3, 1, 3 or 10 mg kg^{-1}, s.c.) and placed in a new observation cage. An overhead camera (GoPro HERO9 at 120 Hz) recorded their movements. Observers scored HTR from recorded footage for the first 10-min period.

Chronic SD stress assay

The current set of experiments used the chronic SD stress paradigm to evaluate the antidepressant efficacy of the compounds of interest[41]. In brief, male 8-week-old C57BL/6J mice were randomly assigned to either the control or stress condition. Mice in the stress condition were subjected to 10 consecutive days of subordination stress by being placed into the territorialized cage of a larger, aggressive CD-1 mouse. Stressed-exposed mice were housed overnight in the compartment adjacent to the recently encountered CD-1 mouse and introduced to a new aggressor each day for a 10-min defeat bout. Control mice were housed in pairs, one on each side of a perforated Plexiglas partition, and handled daily.

SI test

Twenty-four hours after the last defeat bout, mice were tested in the SI test to evaluate stress-induced social avoidance. For this experiment, 1 h after the last defeat bout (day 10), mice were injected with 4-F,5-MeO-PyrT (1.0 mg kg^{-1}) or vehicle and evaluated in the SI test 24 h later. Mice were all randomly assigned to receive either drug or vehicle.

The SI test is a two-session test consisting of a target and no-target session. In the no-target session, the experimental mouse is allowed to explore an open-field arena for 2.5 min. The mouse is then removed, and a new CD-1 male mouse is placed into a wire mesh cage, which is situated along one side of the arena. This area is the interaction zone. For the target session (SI phase), the test mouse is placed back into the arena for another 2.5 min and the amount of time spent in the interaction zone is measured. Experimenters were blinded to the drug pretreatment and behaviour during the SI test, which was automatically tracked using EthoVision analysis software (Noldus). We also calculated the ratio of time spent in the corners of the chamber during the SI phase. Socially defeated mice explored the interaction zone significantly less in the presence of the CD-1 mouse. Data are presented as the IR of time spent in the interaction zone between the target and no-target sessions, and locomotion data were measured during the no-target session. Data were averaged from

three independent experiments. A total of 46 mice were administered vehicle treatment (17 control, 29 stress), 53 received 4-F,5-MeO-PyrT (17 control, 36 stress), 15 received WAY-100635 (5 control, 10 stress), and 29 received 4-F,5-MeO-PyrT + WAY-100635 (10 control, 19 stress). More animals were used for the stressed groups owing to the inherent resilience of mice to SD stress[42]. Analysis of different treatment conditions of control and stressed animals was done using GraphPad Prism with two-way analysis of variance. The interaction of all treatments with control and stressed animals showed a $P = 0.1778$, with a row (treatment) factor of $P = 0.0741$ and a column (control/stress) factor of $P = 0.0001$. Comparison of individual treatments, as shown in Fig. 5d, was done using multiple comparison post hoc analysis using Fisher's least significant difference test. We additionally analysed our data taking into account that a proportion of mice are resilient in this paradigm. Accordingly, we used a Fisher's exact test to analyse and compare the number of mice that are resilient (SI ratio > 1) and susceptible (SI ratio < 1) in the vehicle-treated and 4-F,5-MeO-PyrT-treated stressed cohorts.

Sucrose preference test

The sucrose preference test is a volitional two-bottle choice procedure in which mice are given the choice between consuming water and a 1% sucrose solution. This paradigm has been extensively used to assess the effects of stress-induced anhedonia. On day 10, chronic SD stressed mice were individually housed and habituated to two bottles containing just water. Twenty-four hours later, following the SI test, one bottle was replaced with a 1% sucrose solution (w/v) made with water from the animal vivarium. Mice had ad libitum overnight access to both bottles, and preference for sucrose over water was calculated as follows: (sucrose/(sucrose + water)) × 100. Data were averaged from two independent experiments. A total of 27 mice were administered vehicle (9 control, 18 stress), 27 received 4-F,5-MeO-PyrT (9 control, 18 stress), 15 received WAY-100635 (5 control, 10 stress), and 15 received 4-F,5-MeO-PyrT + WAY-100635 (5 control, 10 stress). More animals were used for the stressed groups owing to the inherent resilience of mice to SD stress[42]. Analysis of different treatment conditions of control and stressed animals was done using GraphPad Prism with two-way analysis of variance. The interaction of all treatments with control and stressed animals showed $P = 0.0773$, with a row (treatment) factor of $P = 0.0159$ and a column (control/stress) factor of $P = 0.0008$. Comparison of individual treatments, as shown in Fig. 5e, was done using multiple comparison post hoc analysis using Fisher's least significance difference test.

Reporting summary

Further information on research design is available in the Nature Portfolio Reporting Summary linked to this article.

Extended Data

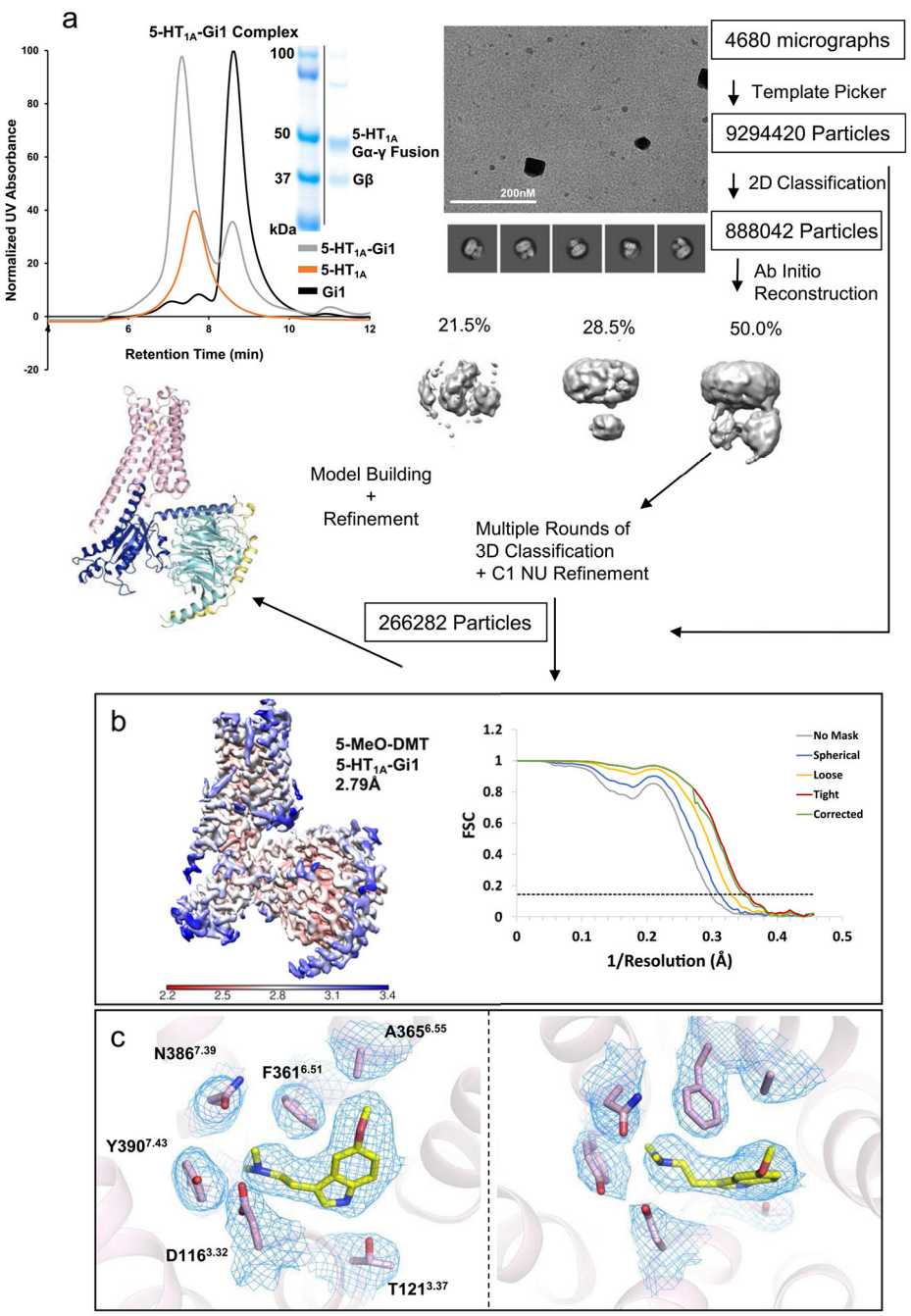

Extended Data Fig. 1 |. Cryo-EM structure determination of drug-bound 5-HT$_{1A}$-Gαi1/Gβ1/Gβ2 complexes.

a, Representative structure determination of 5-MeO-DMT-bound 5-HT$_{1A}$ signalling complex. **Top Left**, Analytical size exclusion chromatography and SDS-PAGE show monodisperse and pure protein of intact complex and its components. **Right**, representative Cryo-EM micrograph (white bar indicates scale) of 4680 total micrographs and data processing schematic exemplified by 5-MeO-DMT-bound 5-HT$_{1A}$-Gi1 structure: After

particle picking, 2D classification and multiple rounds of 3D classification, the final particle stack was refined using non-uniform refinement. A final map was obtained and resolutions were estimated applying the 0.143 cutoff in GS-FSC. Initial models were built in COOT, and then further refined in PHENIX for the generation of final coordinates shown in this manuscript. **b**, Local resolution map of a 5-MeO-DMT-bound 5-HT_{1A}-Gi1 complex (**left**) and FSC curves (**right**) calculated based on the final reconstruction in cryoSPARC. **c**, 5-MeO-DMT (yellow) in the orthosteric binding pocket from the side (**left**) and rotated 45° towards the top of the receptor (**right**) with the map of ligand and surround residue densities shown at 5σ.

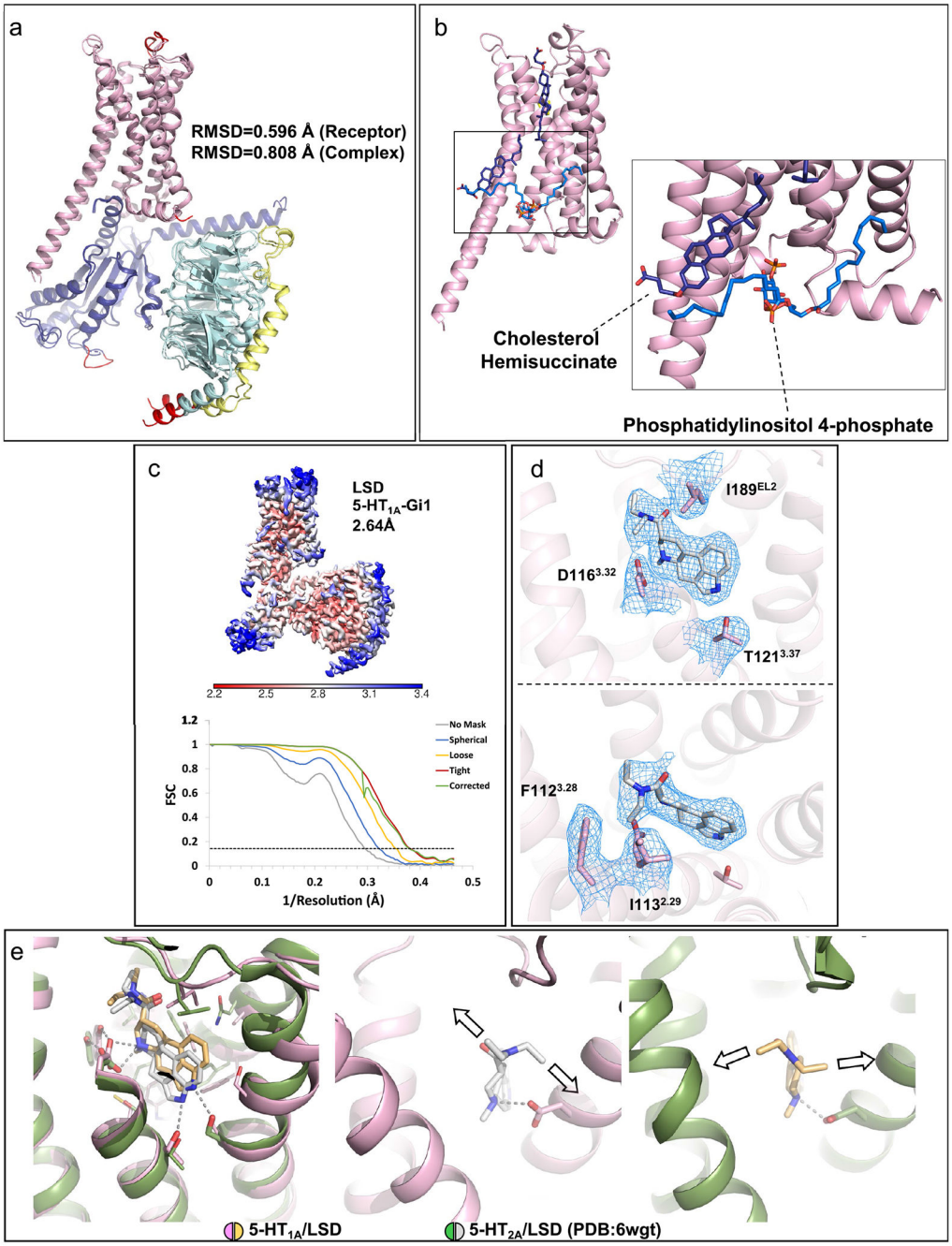

Extended Data Fig. 2 |. Comparison of different 5-HT$_{1A}$ structures and differences in binding of LSD to 5-HT$_{1A}$ and 5-HT$_{2A}$.

a, Superposition of herein reported 5-MeO-DMT-bound 5-HT$_{1A}$-Gi complex with the previously reported 5-HT-bound 5-HT$_{1A}$-Gi structure (PDB ID: 7E2Y) shows similar conformations. Additional residues in 5-HT$_{1A}$'s EL2 and G proteins not observed in previous structures are highlighted in red. **b**, Lipids (blue) and cholesterol hemisuccinate (dark blue) are bound to similar sites as observed before. **c**, Local resolution map of a LSD-bound 5-HT$_{1A}$-Gi1 complex (**left**) and FSC curves (**right**) calculated the final

reconstruction in cryoSPARC. **d**, LSD (grey) in the orthosteric binding pocket from the side (**top**) and rotated 45° towards the top of the receptor (**bottom**) with the map of ligand and surround residue densities shown at 5σ. **e**, LSD shows distinct binding modes bound to 5-HT_{1A}-Gi signalling complex and 5-HT_{2A} (PDB ID: 6WGT). **Left**, 5-HT_{1A}-bound LSD (grey) sits deeper in the binding pocket compared to 5-HT_{2A}-bound LSD (orange). Zoom in of LSD in 5-HT_{1A}-Gi structure (**middle**) and 5-HT_{2A} structure (**right**) highlights differential stereochemistry and receptor-specific interactions of diethylamide moiety. Hydrogen bonds are indicated as grey dashed lines.

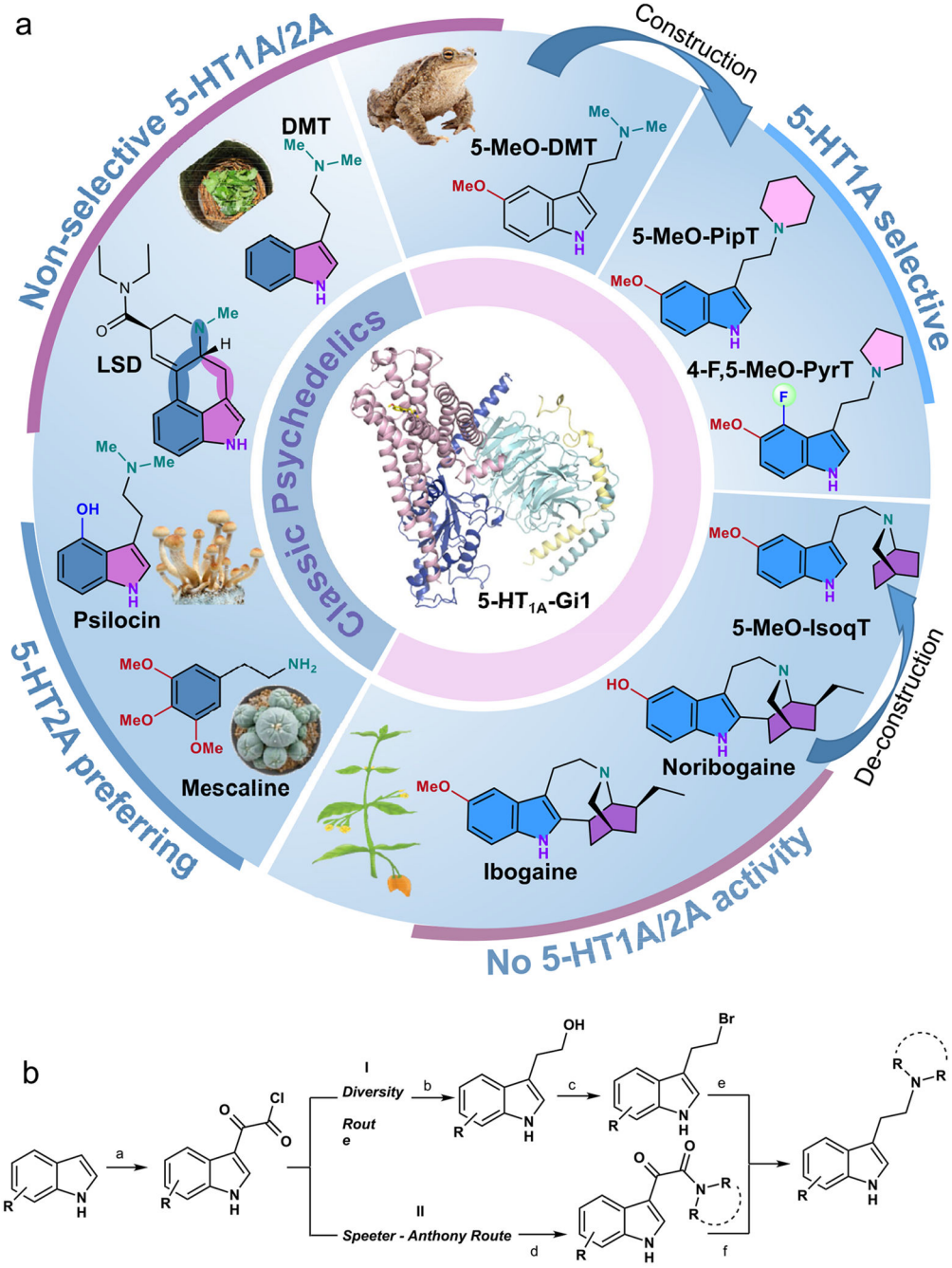

Extended Data Fig. 3 |. Global structure-activity landscape of tryptamine psychedelics at 5-HT$_{1A}$ and 5-HT$_{2A}$ receptors and their synthesis.

a, Overview of the cryo-EM structure of the 5HT$_{1A}$ receptor-Gi signalling complex bound to 5-MeO-DMT (**center**). Classic psychedelics such as the prototypical compounds DMT and LSD are agonists of both 5-HT$_{1A}$ and 5-HT$_{2A}$ receptors (**left semicircle**). 5-MeO-DMT (**top ofthe circle**), a major psychoactive compound found in toad secretions, shows comparable potency and efficacy at both 5-HT$_{1A}$ and 5-HT$_{2A}$ receptors. Systematic structural mapping via elaboration of the core 5-MeO-DMT structure identifies a class of 5-MeO-tryptamines

with increasing 5-HT_{1A} selectivity (**right hemi-circle**). 5-MeO-DMT can be viewed as a deconstruction of ibogaine, a oneirogen with a complex polycyclic tryptamine structure (**bottom ofthe circle**). Iboga compounds show no activity at 5-HT_{1A} and 5-HT_{2A} receptors, but this activity re-emerges by deconstruction of the isoquinuclidine core to simple mono-cyclic tryptamines such as 5-MeO-PipT (5-methoxypiperidinyl-tryptamine) and 4-F,5-MeO-PyrT (4-fluoro, 5-methoxypyrrolidinyl-tryptamine, right hemi-circle). Images of peyote, mushrooms, ayahuasca, and toad are from iStock and ShutterStock, and *Tabernanthe iboga* schematic is adapted from previous work[65]. **b**, General synthesis methodology of tryptamines. a. oxalyl chloride, b. MeOH, LAH, c. PPh3, CBr4, d. Amine, TEA, e. Amine, f. LAH.

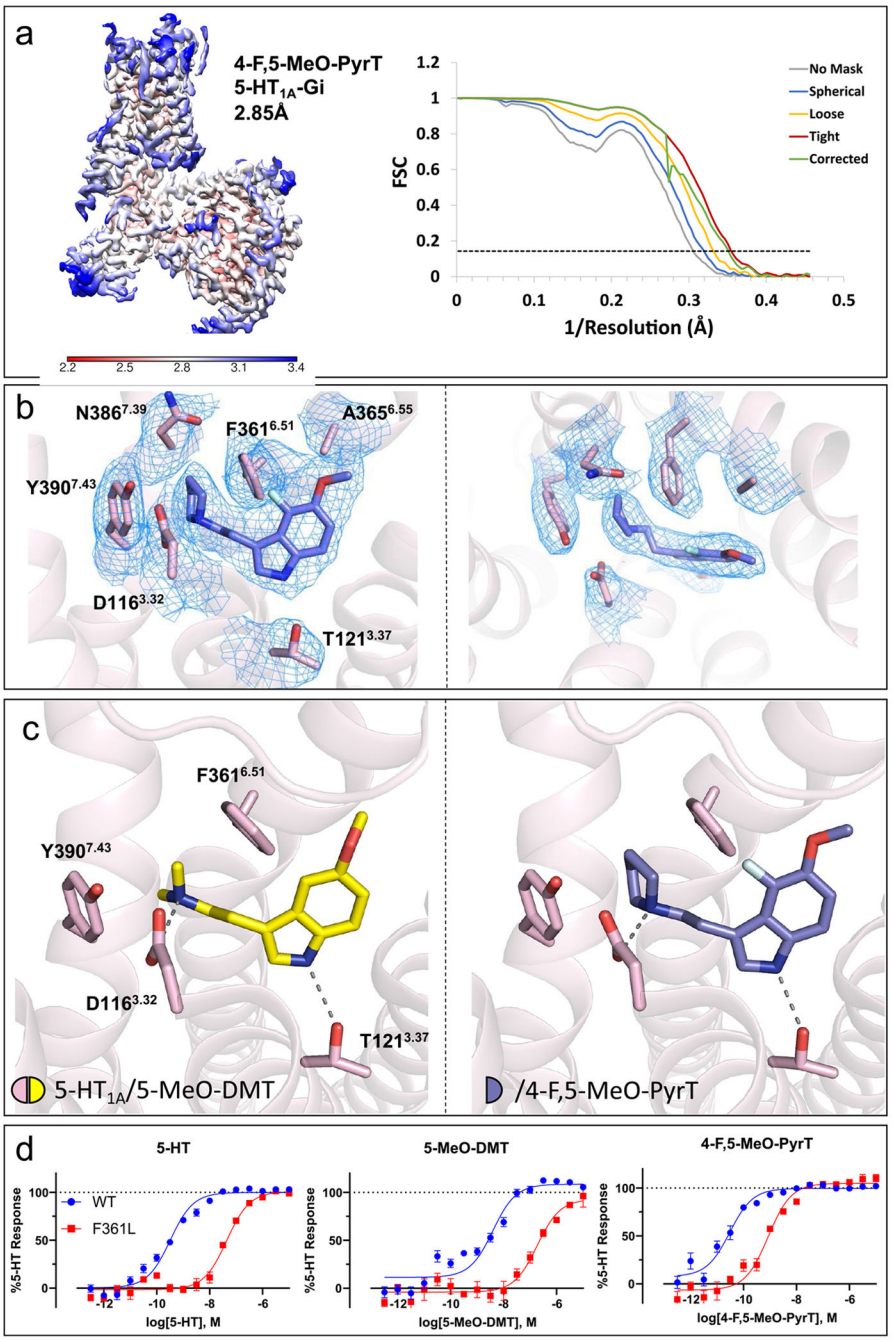

Extended Data Fig. 4 |. Structural comparison of 5-MeO-DMT 5-HT1A-selective analog 4-F, 5-MeO-PyrT bound to 5-HT$_{1A}$.

a, Local resolution map of a 4-F,5-MeO-PyrT-bound 5-HT$_{1A}$-Gi1 complex (**left**) and FSC curves (**right**) calculated from the final reconstruction in cryoSPARC. **b**, 4-F,5-MeO-PyrT (dark blue) in the orthosteric binding pocket from the side (**left**) and rotated 45° towards the top of the receptor (**right**) with the map of ligand and surrounding residue densities shown at 5σ. **c**, structural side-by-side comparison of 5-HT$_{1A}$ orthosteric site bound to 5-MeO-DMT (yellow) and 4-F,5-MeO-PyrT (dark blue). **d**, cAMP accumulation assays using

wildtype and mutant 5-HT$_{1A}$, and different drugs. Concentration-response experiments reveal different sensitivities of distinct drugs to F361L mutation. All signalling studies were performed in triplicates and are averaged from two to three independent experiments. Data have been normalized against 5-HT and errors bars denote s.e.m.

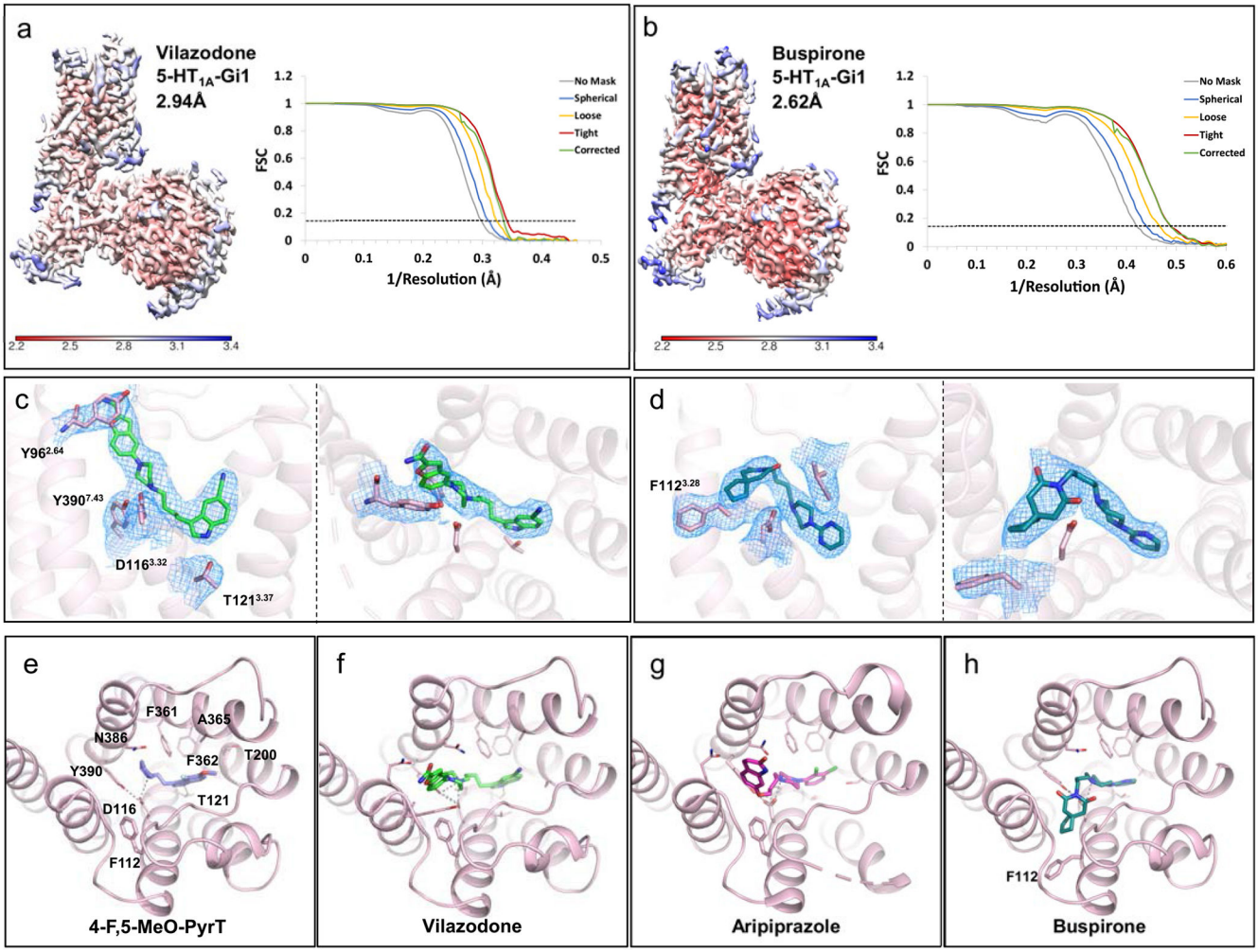

Extended Data Fig. 5 |. Comparison of 4-F,5-MeO-PyrT binding pose to that of different clinical 5-HT$_{1A}$ drugs.

a, **b**, Local resolution maps of vilazodone-bound (**a**) and buspirone-bound (**b**) 5-HT$_{1A}$-Gi1 complexes and corresponding FSC curves calculated from the final reconstructions in cryoSPARC. **c**, **d**, Vilazodone (**c**, green) and buspirone (**d**, teal) in the orthosteric binding pocket from the side (**left**) and rotated 45° towards the top of the receptor (**right**) with the density map of ligand and surrounding residues shown at 5σ. **e-h**, Extracellular view of 4-F,5-MeO-PyrT (**e**, dark blue), Vilazodone (**f**, green), Aripiprazole (**g**, magenta, PDB ID: 7E2Z), and Buspirone (**h**, teal) binding poses in 5-HT$_{1A}$'s orthosteric site.

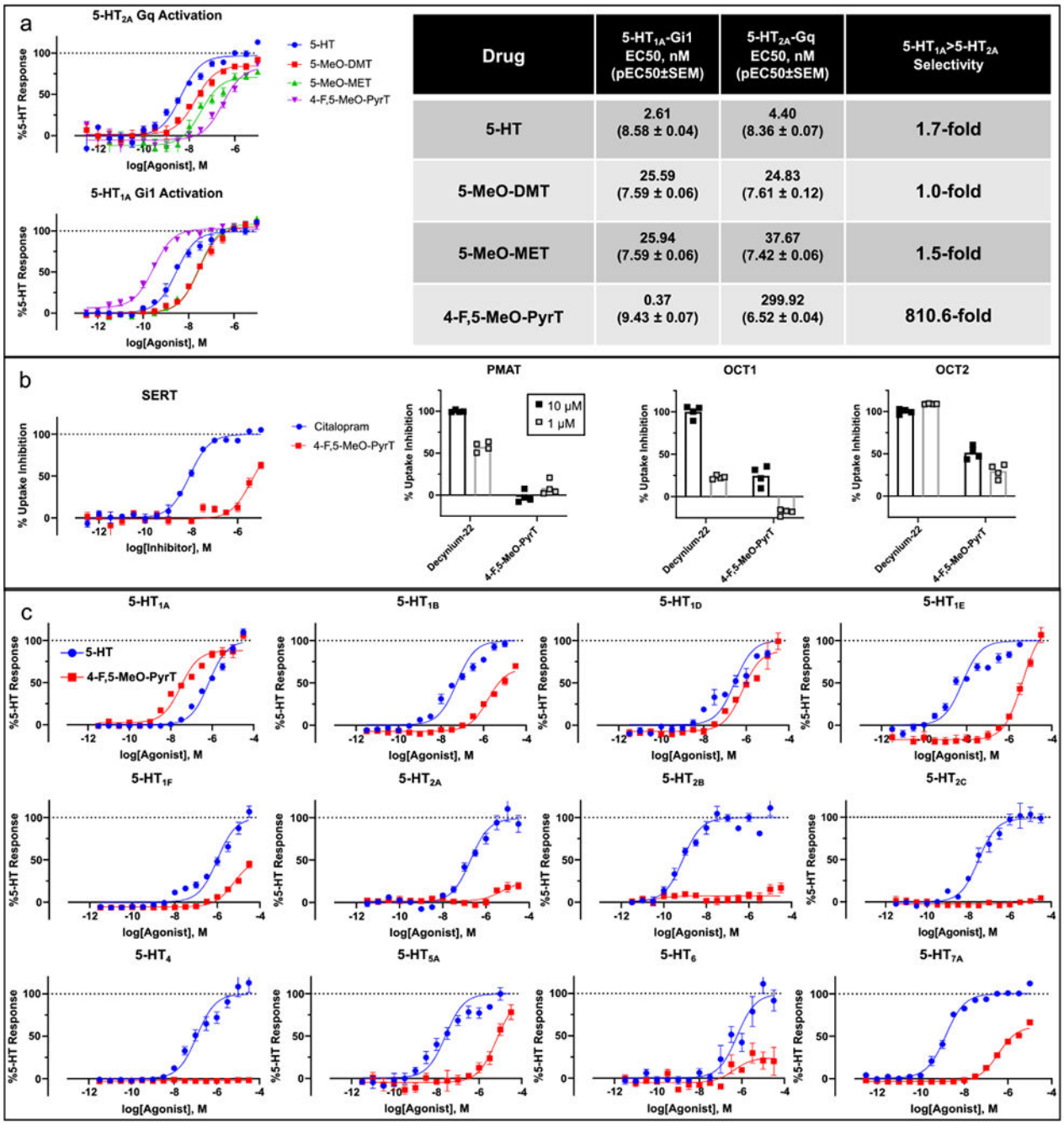

Drug	5-HT$_{1A}$-Gi1 EC50, nM (pEC50±SEM)	5-HT$_{2A}$-Gq EC50, nM (pEC50±SEM)	5-HT$_{1A}$>5-HT$_{2A}$ Selectivity
5-HT	2.61 (8.58 ± 0.04)	4.40 (8.36 ± 0.07)	1.7-fold
5-MeO-DMT	25.59 (7.59 ± 0.06)	24.83 (7.61 ± 0.12)	1.0-fold
5-MeO-MET	25.94 (7.59 ± 0.06)	37.67 (7.42 ± 0.06)	1.5-fold
4-F,5-MeO-PyrT	0.37 (9.43 ± 0.07)	299.92 (6.52 ± 0.04)	810.6-fold

Extended Data Fig. 6 |. Selectivity of different 5-MeO-DMT analogs and off-target activity of 4-F,5-MeO-PyrT.

a, 5-HT$_{1A}$-Gi and 5-HT$_{2A}$-Gq BRET of 5-HT, 5-MeO-DMT, 5-MeO-MET, and 4-F,5-MeO-PyrT with respective potencies and 5-HT$_{1A}$ >5-HT$_{2A}$ selectivities. **b**, Off-target inhibition of transporters SERT, PMAT, OCT1, and OCT2 by 4-F,5-MeO-PyrT and known inhibitors. SERT uptake was performed in triplicates and data was averaged from two independent experiments showing data as mean+s.e.m. PMAT, OCT1, and OCT2 uptake was performed once in quadruplicate. c, Arrestin-recruitment of 5-HT and 4-F,5-MeO-PyrT at all human

5-HT receptor subtypes except for 5-HT_{7A}, whose activation was measured via cAMP stimulation. All functional studies were performed in triplicates and are averaged from two to three independent experiments. Data have been normalized against 5-HT, Citalopram, and Decynium-22, and errors bars denote the s.e.m.

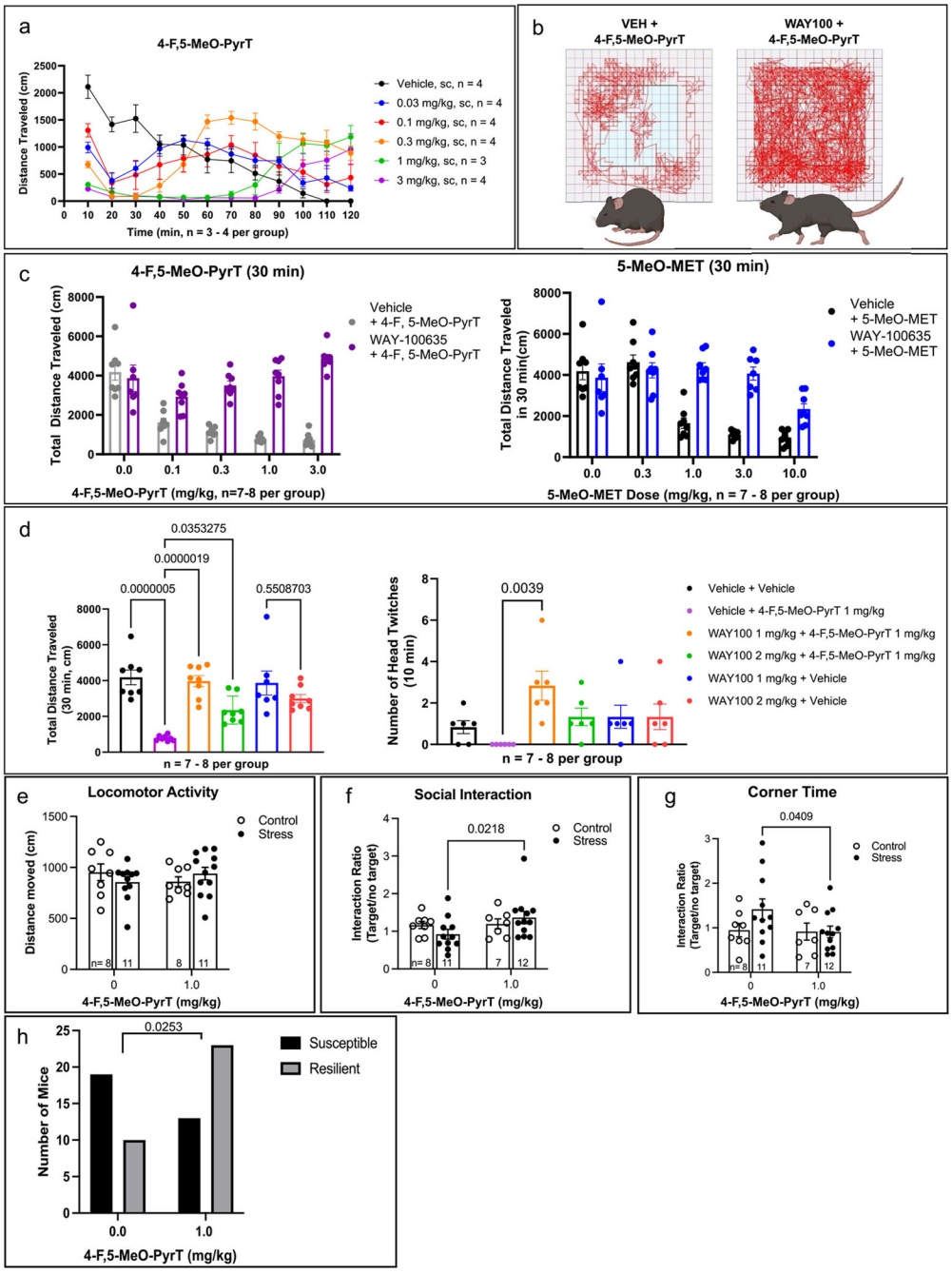

Extended Data Fig. 7 |. Effects of 5-MeO-DMT derivatives on rodent behavior.
a, Evaluation of 4-F,5-MeO-PyrT in open field for two hours (n = 3-4/group). **b**, Exemplary traces of the ambulatory distance traveled in open field following 4-F,5-MeO-PyrT (1 mg/kg,

s.c.) administration and with and without WAY-100635 pre-treatment (1 mg/kg, s.c., 15 min prior). Panel was created with BioRender.com. **c**, Effect of WAY-100635 (1 mg/kg, s.c., 15 min prior) on 4-F,5-MeO-PyrT's and 5-MeO-MET's effect on total locomotion (n = 7-8/group, 30 min). **d**, Determination of optimal inhibitory WAY-100635 dose via administration of 1 mg/kg and 2 mg/kg WAY-100635 prior to studying 4-F,5-MeO-PyrT's effects on total locomotion (n = 7 - 8/group) and HTR (n = 6/group). Analysis was done using one-way ANOVA with multiple comparisons with Tukey's post hoc test, and exact p values have been denoted in the Figure. **e-g**, Effects of saline or 4-F,5-MeO-PyrT administration on control (Control) or chronically defeated mice (Stress). Determination of **e**, distance moved as a measure of locomotor activity, **f**, social interaction as a measure of anxiety- and depression-related phenotype, **g**, corner time as a measure of anxiety-like behavior. Analysis was done in a sub-cohort of the animals reported in Fig. 5d. Number of mice for each group is indicated below the data for each respective cohort. Differences were determined by two-way ANOVA with multiple comparisons using Fisher's LSD post hoc test, and exact p values have been denoted in the Figure. **h**, Vehicle- and drug-treated stressed mice shown in Fig. 5d were divided into susceptible (SI ratio<1) and resilient (SI ratio>1) populations. Significance in the population shift was determined by a twosided Fisher's exact test and p value and number of mice have been denoted in the Figure. Error bars denote the s.e.m.

Extended Data Table 1|

Cryo-EM Data Collection, Model Refinement and Validation

	5-HT1A Gi1 DNG 5-MeO-DMT	**5-HT1A Gi1 LSD**	**5-HT1A Gi1 4-F, 5-MeO-PyrT**	**5-HT1A Gi1 Vilazodone**	**5-HT1A Gi1 DNG Buspirone**
Data Collection and Processing					
Magnification	64000	81000	64000	81000	105000
Voltage (kV)	300	300	300	300	300
Electron Exposure (e-/A2)	52.13	53.61	52.23	54.3	50
Defocus Range (μm)	−0.5 to −1.8	−0.5 to −1.8	−0.5 to −1.8	−0.5 to −1.8	−0.5 to −1.8
Pixel Size	1.076	1.058	1.076	1.069	0.825
Symmetry Imposed	C1	C1	C1	C1	C1
Total Micrographs	4680	4952	3071	7206	2489
Initial Particle Images	9294420	12502189	4565297	18088270	4167166
Final Particle Images	266282	318050	265975	785536	586489
Map Resolution	2.79	2.64	2.85	2.94	2.62
FSC Threshold	0.143	0.143	0.143	0.143	0.143
Sharpening B-factor	120.5	91.6	110.2	167.3	105.1
Refinement					
Model Composition					
Non-hydrogen Atoms	7309	7321	7321	7330	7325

	5-HT1A Gi1 DNG 5-MeO-DMT	5-HT1A Gi1 LSD	5-HT1A Gi1 4-F, 5-MeO-PyrT	5-HT1A Gi1 Vilazodone	5-HT1A Gi1 DNG Buspirone
Protein Residues	914	914	914	914	914
Ligands	4	4	4	4	4
RMS Deviations					
Bond Lengths (Å)	0.008	0.005	0.004	0.004	0.005
Bond Angles (°)	1.161	0.686	0.630	0.593	1.030
Clash Score	5.35	5.75	6.10	5.14	6.71
Rotamers Outliers (%)	0.13	0	0	0	0
Ramachandran Plot (%)					
Favored	97.45	97.78	97.67	98.12	97.45
Allowed	2.55	2.22	2.33	1.88	2.55
Outliers	0	0	0	0	0
Data Availability					
PDB	8FY8	8FYT	8FYE	8FYL	8FYX
EMDB	EMD-29560	EMD-29597	EMD-29571	EMD-29585	EMD-29599

Report of data collection and refinement statistics from the structures presented in the manuscript. DNG indicates use of a dominant negative G protein further described in the methods.

Extended Data Table 2|

AUClast and Cmax of 4-F,5-MeO-PyrT at 1 mg/kg SC administration, and Plasma and Brain Tissue Binding of 4-F,5-MeO-PyrT

Pharmacokinetics			
Tissue	**AUC_{last} (hr*ng/mL)**	**Tissue**	**Cmax (ng/mL)**
Plasma	26.40	Plasma	44.02
Brain	128.34	Brain	143.35

Mouse Brain Tissue Binding										
Sr.no	**Compound**	**Species**	**% Bound**			**STDV**	**% Unbound**	**fu**	**% Recovery**	**% Compound remaining at 4 h**
			R1	**R2**	**Mean**					
1	Carbamazepine	Mouse Brain	89.0	87.4	88.2	1.1	11.8	0.118	72	96
2	4-F, 5-MeO-PyrT		84.3	80.7	82.5	2.5	17.5	0.175	88	96
Mouse Plasma Protein Binding										
1	Warfarin	Mouse Plasma	93.9	93.3	93.6	0.4	6.4	0.064	90.9	103.3
2	4-F, 5-MeO-PyrT		32.04	42.68	37.36	7.5	62.64	0.626	84.7	105.6
Human Plasma Protein Binding										

Mouse Brain Tissue Binding										
Sr.no	Compound	Species	% Bound			STDV	% Unbound	fu	% Recovery	% Compound remaining at 4 h
			R1	R2	Mean					
1	Warfarin	Human Plasma	98.0	98.5	98.3	0.3	1.7	0.017	108.1	108.8
2	4-F, 5-MeO-PyrT		22.19	29.83	26.01	5.4	73.99	0.740	81.8	97.9

Summary of the pharmacokinetic and in vivo binding properties of 4-F,5-MeO-PyrT.

Supplementary Material

Refer to Web version on PubMed Central for supplementary material.

Acknowledgements

This work was supported by NIH grant R35GM133504, a Sloan Research Fellowship in Neuroscience, an Edward Mallinckrodt, Jr Foundation Grant, a McKnight Foundation Scholars Award, an Irma T. Hirschl/Monique Weill-Caulier Trust Research Award (all to D.W.); an NIH F31 MH132317 (A.L.W), and T32 Training Grant GM062754 and DA053558 (A.L.W and G.Z.); the G. Harold & Leila Y. Mathers Charitable Foundation, the NIH grant R01DA050613, G.L. Freeman, and Columbia University for support of this work (all to D.S.); and the following NIH grants: R01MH127820 and R01MH104559 (S.J.R.). L.F.P is supported by the Leon Levy Foundation and the Brain and Behavior Research Foundation. Some of this work was performed at the National Center for CryoEM Access and Training (NCCAT) and the Simons Electron Microscopy Center located at the New York Structural Biology Center, supported by the NIH Common Fund Transformative High Resolution Cryo-Electron Microscopy program (U24 GM129539) and by grants from the Simons Foundation (SF349247) and NY State Assembly. We further acknowledge cryo-EM resources at the National Resource for Automated Molecular Microscopy located at the New York Structural Biology Center, supported by grants from the Simons Foundation (SF349247), NYSTAR, and the NIH National Institute of General Medical Sciences (GM103310) with additional support from Agouron Institute (F00316) and NIH (OD019994). For additional data collection, we are grateful to staff at the Laboratory for BioMolecular Structure (LBMS), which is supported by the DOE Office of Biological and Environmental Research (KP160711). This work was supported in part through the computational and data resources and staff expertise provided by Scientific Computing and Data at the Icahn School of Medicine at Mount Sinai and supported by the Clinical and Translational Science Awards (CTSA) grant ULTR004419 from the National Center for Advancing Translational Sciences. We thank B.Bechand for early examination of in vivo pharmacology of the described compounds assisted by V.C. Galicia; C. Hwu for assistance with synthesis and purification of several compounds (all at Columbia University); and F. Zandkarimi from the Columbia University Chemistry Department Mass Spectrometry Core Facility for conducting the high-resolution mass spectrometry experiments.

Data availability

Density maps and structure coordinates have been deposited into the Electron Microscopy Data Bank (EMDB) and the PDB with the following accession identifiers: EMD-29560 and PDB 8FY8 for 5-MeO-DMT–5-HT_{1A}–$G\beta_{i1}$–$G\beta_1$–$G\gamma_2$; EMD-29597 and PDB 8FYT for LSD–5-HT_{1A}–$G\alpha_{i1}$–$G\beta_1$-$G\gamma_2$; EMD-29571 and PDB 8FYE for 4-F,5-MeO-PyrT–5-HT_{1A}–$G\alpha_{i1}$–$G\beta_1$–$G\gamma_2$; EMD-29585 and PDB 8FYL for vilazodone–5-HT_{1A}–$G\alpha_{i1}$–$G\beta_1$-$G\gamma_2$; and EMD-29599 and PDB 8FYX for buspirone–5-HT_{1A}–$G\alpha_{i1}$–$G\beta_1$–$G\gamma_2$. Source data are provided with this paper. Additional data from this study are available upon request.

References

1. Carhart-Harris RL et al. Psilocybin with psychological support for treatment-resistant depression: six-month follow-up. Psychopharmacology 235, 399–408 (2018). [PubMed: 29119217]
2. Armstrong SB et al. Prospective associations of psychedelic treatment for co-occurring alcohol misuse and posttraumatic stress symptoms among United States Special Operations Forces veterans. Mil. Psychol 10.1080/08995605.2022.2156200 (2023).

3. Goodwin GM et al. Single-dose psilocybin for a treatment-resistant episode of major depression. N. Engl. J. Med 387, 1637–1648 (2022). [PubMed: 36322843]
4. Cameron LP et al. 5-HT_{2A}Rs mediate therapeutic behavioral effects of psychedelic tryptamines. ACS Chem. Neurosci 10.1021/acschemneuro.2c00718 (2023).
5. Krebs-Thomson K, Ruiz EM, Masten V, Buell M, & Geyer MA The roles of 5-HT_{1A} and 5-HT_2 receptors in the effects of 5-MeO-DMT on locomotor activity and prepulse inhibition in rats. Psychopharmacology 189, 319–329 (2006). [PubMed: 17013638]
6. Schwelm HM et al. Qualitative and quantitative analysis of tryptamines in the poison of *Incilius alvarius* (Amphibia: Bufonidae). J. Anal. Toxicol 46, 540–548 (2022). [PubMed: 33851996]
7. Hughes ZA et al. Neurochemical evaluation of the novel 5-HT_{1A} receptor partial agonist/serotonin reuptake inhibitor, vilazodone. Eur. J. Pharmacol 510, 49–57 (2005). [PubMed: 15740724]
8. Loane C & Politis M Buspirone: what is it all about? Brain Res. 1461, 111–118 (2012). [PubMed: 22608068]
9. Winter JC, Filipink RA, Timineri D, Helsley SE & Rabin RA The paradox of 5-methoxy-*N,N*-dimethyltryptamine: an indoleamine hallucinogen that induces stimulus control via 5-HT1A receptors. Pharmacol. Biochem. Behav. 65, 75–82 (2000). [PubMed: 10638639]
10. Davis AK, So S, Lancelotta R, Barsuglia JP & Griffiths RR 5-Methoxy-*N,N*-dimethyltryptamine (5-MeO-DMT) used in a naturalistic group setting is associated with unintended improvements in depression and anxiety. Am. J. Drug Alcohol Abuse 45, 161–169 (2019). [PubMed: 30822141]
11. Reckweg JT et al. The clinical pharmacology and potential therapeutic applications of 5-methoxy-*N,N*-dimethyltryptamine (5-MeO-DMT). J. Neurochem 162, 128–146 (2022). [PubMed: 35149998]
12. Chauhan M, Parry R & Bobo WV Vilazodone for major depression in adults: pharmacological profile and an updated review for clinical practice. Neuropsychiatr. Dis. Treat. 18, 1175–1193 (2022). [PubMed: 35726313]
13. Kim K et al. Structure of a hallucinogen-activated Gq-coupled 5-HT_{2A} serotonin receptor. Cell 182, 1574–1588.e19 (2020). [PubMed: 32946782]
14. Wacker D et al. Crystal structure of an LSD-bound human serotonin receptor. Cell 168, 377–389.e12 (2017). [PubMed: 28129538]
15. Cameron LP et al. A non-hallucinogenic psychedelic analogue with therapeutic potential. Nature 589, 474–479 (2021). [PubMed: 33299186]
16. Kaplan AL et al. Bespoke library docking for 5-HT_{2A} receptor agonists with antidepressant activity. Nature 610, 582–591 (2022). [PubMed: 36171289]
17. Carhart-Harris RL & Nutt DJ Serotonin and brain function: a tale of two receptors. J. Psychopharmacol. 31, 1091–1120 (2017). [PubMed: 28858536]
18. Olsen RHJ et al. TRUPATH, an open-source biosensor platform for interrogating the GPCR transducerome. Nat. Chem. Biol. 16, 841–849 (2020). [PubMed: 32367019]
19. Nichols DE Chemistry and structure–activity relationships of psychedelics. Curr. Top. Behav. Neurosci. 36, 1–43 (2018).
20. Glennon RA et al. Binding of β-carbolines and related agents at serotonin (5-HT_2 and 5-HT_{1A}), dopamine (D_2) and benzodiazepine receptors. Drug Alcohol Depend. 60, 121–132 (2000). [PubMed: 10940539]
21. Halberstadt AL & Geyer MA Multiple receptors contribute to the behavioral effects of indoleamine hallucinogens. Neuropharmacology 61, 364–381 (2011). [PubMed: 21256140]
22. Xu P et al. Structural insights into the lipid and ligand regulation of serotonin receptors. Nature 592, 469–473 (2021). [PubMed: 33762731]
23. Ballesteros JA & Weinstein H Integrated methods for the construction of three-dimensional models and computational probing of structure–function relations in G protein-coupled receptors. Methods Neurosci. 25, 366–428 (1995).
24. Rasmussen SG et al. Crystal structure of the β_2 adrenergic receptor–Gs protein complex. Nature 477, 549–555 (2011). [PubMed: 21772288]
25. Wacker D et al. Structural features for functional selectivity at serotonin receptors. Science 340, 615–619 (2013). [PubMed: 23519215]

26. Nichols DE, Monte A, Huang X & Marona-Lewicka D Stereoselective pharmacological effects of lysergic acid amides possessing chirality in the amide substituent. Behav. Brain Res. 73, 117–119 (1996). [PubMed: 8788487]
27. Speeter ME & Anthony WC The action of oxalyl chloride on indoles—a new approach to tryptamines. J. Am. Chem. Soc. 76, 6208–6210 (1954).
28. Shulgin AT & Shulgin A Tihkal: The Continuation (Transform Press, 1997).
29. Kozell LB et al. Pharmacologic activity of substituted tryptamines at 5-hydroxytryptamine (5-HT)$_{2A}$ receptor (5-HT$_{2A}$R), 5-HT$_{2C}$R, 5-HT$_{1A}$R, and serotonin transporter. J. Pharmacol. Exp. Ther. 385, 62–75 (2023). [PubMed: 36669875]
30. Blair JB et al. Effect of ring fluorination on the pharmacology of hallucinogenic tryptamines. J. Med. Chem 43, 4701–4710 (2000). [PubMed: 11101361]
31. Laban U, Kurrasch-Orbaugh D, Marona-Lewicka D & Nichols DE A novel fluorinated tryptamine with highly potent serotonin 5-HT$_{1A}$ receptor agonist properties. Bioorg. Med. Chem. Lett 11, 793–795 (2001). [PubMed: 11277522]
32. Wang C et al. Structural basis for molecular recognition at serotonin receptors. Science 340, 610–614 (2013). [PubMed: 23519210]
33. Gasser P, Kirchner K & Passie T LSD-assisted psychotherapy for anxiety associated with a life-threatening disease: a qualitative study of acute and sustained subjective effects. J. Psychopharmacol. 29, 57–68 (2015). [PubMed: 25389218]
34. Halberstadt AL, Koedood L, Powell SB & Geyer MA Differential contributions of serotonin receptors to the behavioral effects of indoleamine hallucinogens in mice. J. Psychopharmacol 25, 1548–1561 (2011). [PubMed: 21148021]
35. Darmani NA, Martin BR, Pandey U & Glennon RA Do functional relationships exist between 5-HT$_{1A}$ and 5-HT$_2$ receptors. Pharmacol. Biochem. Behav 36, 901–906 (1990). [PubMed: 2145593]
36. Arnt J & Hyttel J Facilitation of 8-OHDPAT-induced forepaw treading of rats by the 5-HT$_2$ agonist DOI. Eur. J. Pharmacol 161, 45–51 (1989). [PubMed: 2524390]
37. Ermakova AO, Dunbar F, Rucker J & Johnson MW A narrative synthesis of research with 5-MeO-DMT. J. Psychopharmacol 36, 273–294 (2022). [PubMed: 34666554]
38. Bagot RC et al. Ketamine and imipramine reverse transcriptional signatures of susceptibility and induce resilience-specific gene expression profiles. Biol. Psychiatry 81, 285–295 (2017). [PubMed: 27569543]
39. Berton O et al. Essential role of BDNF in the mesolimbic dopamine pathway in social defeat stress. Science 311, 864–868 (2006). [PubMed: 16469931]
40. Donahue RJ, Muschamp JW, Russo SJ, Nestler EJ & Carlezon WA Jr. Effects of striatal ΔFosB overexpression and ketamine on social defeat stress-induced anhedonia in mice. Biol. Psychiatry, 76, 550–558 (2014). [PubMed: 24495460]
41. Golden SA, Covington HE 3rd, Berton O & Russo SJ A standardized protocol for repeated social defeat stress in mice. Nat. Protoc 6, 1183–1191 (2011). [PubMed: 21799487]
42. Krishnan V et al. Molecular adaptations underlying susceptibility and resistance to social defeat in brain reward regions. Cell 131, 391–404 (2007). [PubMed: 17956738]
43. Willner P, Towell A, Sampson D, Sophokleous S & Muscat R Reduction of sucrose preference by chronic unpredictable mild stress, and its restoration by a tricyclic antidepressant. Psychopharmacology 93, 358–364 (1987). [PubMed: 3124165]
44. Li N et al. Glutamate *N*-methyl-D-aspartate receptor antagonists rapidly reverse behavioral and synaptic deficits caused by chronic stress exposure. Biol. Psychiatry 69, 754–761 (2011). [PubMed: 21292242]
45. Hesselgrave N, Troppoli TA, Wulff AB, Cole AB & Thompson SM Harnessing psilocybin: antidepressant-like behavioral and synaptic actions of psilocybin are independent of 5-HT2R activation in mice. Proc. Natl Acad. Sci. USA, 10.1073/pnas.2022489118 (2021).
46. Shao LX et al. Psilocybin induces rapid and persistent growth of dendritic spines in frontal cortex *in vivo*. Neuron 109, 2535–2544.e4 (2021). [PubMed: 34228959]
47. de la Fuente Revenga M et al. Prolonged epigenomic and synaptic plasticity alterations following single exposure to a psychedelic in mice. Cell Rep. 37, 109836 (2021). [PubMed: 34686347]

48. Savalia NK, Shao LX & Kwan AC A dendrite-focused framework for understanding the actions of ketamine and psychedelics. Trends Neurosci. 44, 260–275 (2021). [PubMed: 33358035]
49. Bickle JG et al. 5HT$_{1A}$ receptors on dentate gyrus granule cells confer stress resilience. Biol. Psychiatry 10.1016/j.biopsych.2023.10.007 (2023).
50. Newman-Tancredi A et al. NLX-112, a highly selective 5-HT$_{1A}$ receptor agonist, mediates analgesia and antidepressant-like activity in rats via spinal cord and prefrontal cortex 5-HT$_{1A}$ receptors, respectively. Brain Res. 1688, 1–7 (2018). [PubMed: 29555239]
51. Becker AM et al. Ketanserin reverses the acute response to LSD in a randomized, double-blind, placebo-controlled, crossover study in healthy subjects. Int. J. Neuropsychopharmacol 10.1093/ijnp/pyac075 (2022).
52. Strassman RJ Human psychopharmacology of *N,N*-dimethyltryptamine. Behav. Brain Res 73, 121–124 (1996). [PubMed: 8788488]
53. Pokorny T, Preller KH, Kraehenmann R & Vollenweider FX Modulatory effect of the 5-HT$_{1A}$ agonist buspirone and the mixed non-hallucinogenic 5-HT$_{1A/2A}$ agonist ergotamine on psilocybin-induced psychedelic experience. Eur. Neuropsychopharmacol 26, 756–766 (2016). [PubMed: 26875114]
54. Reckweg J. et al. A phase 1, dose-ranging study to assess safety and psychoactive effects of a vaporized 5-methoxy-*N,N*-dimethyltryptamine formulation (GH001) in healthy volunteers. Front. Pharmacol 12, 760671 (2021). [PubMed: 34912222]
55. Shapiro DA et al. Aripiprazole, a novel atypical antipsychotic drug with a unique and robust pharmacology. Neuropsychopharmacology 28, 1400–1411 (2003). [PubMed: 12784105]
56. Zheng SQ et al. MotionCor2: anisotropic correction of beam-induced motion for improved cryo-electron microscopy. Nat. Methods 14, 331–332 (2017). [PubMed: 28250466]
57. Punjani A, Rubinstein JL, Fleet DJ & Brubaker MA cryoSPARC: algorithms for rapid unsupervised cryo-EM structure determination. Nat. Methods 14, 290–296 (2017). [PubMed: 28165473]
58. Punjani A, Zhang H & Fleet DJ Non-uniform refinement: adaptive regularization improves single-particle cryo-EM reconstruction. Nat. Methods 17, 1214–1221 (2020). [PubMed: 33257830]
59. Emsley P, Lohkamp B, Scott WG & Cowtan K Features and development of Coot. Acta Crystallogr. D Biol. Crystallogr 66, 486–501 (2010). [PubMed: 20383002]
60. Liebschner D. et al. Macromolecular structure determination using X-rays, neutrons and electrons: recent developments in Phenix. Acta Crystallogr. D Struct. Biol 75, 861–877 (2019). [PubMed: 31588918]
61. Yamashita K, Palmer CM, Burnley T & Murshudov GN Cryo-EM single-particle structure refinement and map calculation using Servalcat. Acta Crystallogr. D Struct. Biol 77, 1282–1291 (2021). [PubMed: 34605431]
62. The PyMOL Molecular Graphics System v.2.0 (Schrödinger, 2017).
63. Kroeze WK et al. PRESTO-Tango as an open-source resource for interrogation of the druggable human GPCRome. Nat. Struct. Mol. Biol 22, 362–369 (2015). [PubMed: 25895059]
64. Henke A. et al. Toward serotonin fluorescent false neurotransmitters: development of fluorescent dual serotonin and vesicular monoamine transporter substrates for visualizing serotonin neurons. ACS Chem. Neurosci 9, 925–934 (2018). [PubMed: 29281252]
65. Rodriguez P. et al. A single administration of the atypical psychedelic ibogaine or its metabolite noribogaine induces an antidepressant-like effect in rats. ACS Chem. Neurosci 11, 1661–1672 (2020). [PubMed: 32330007]

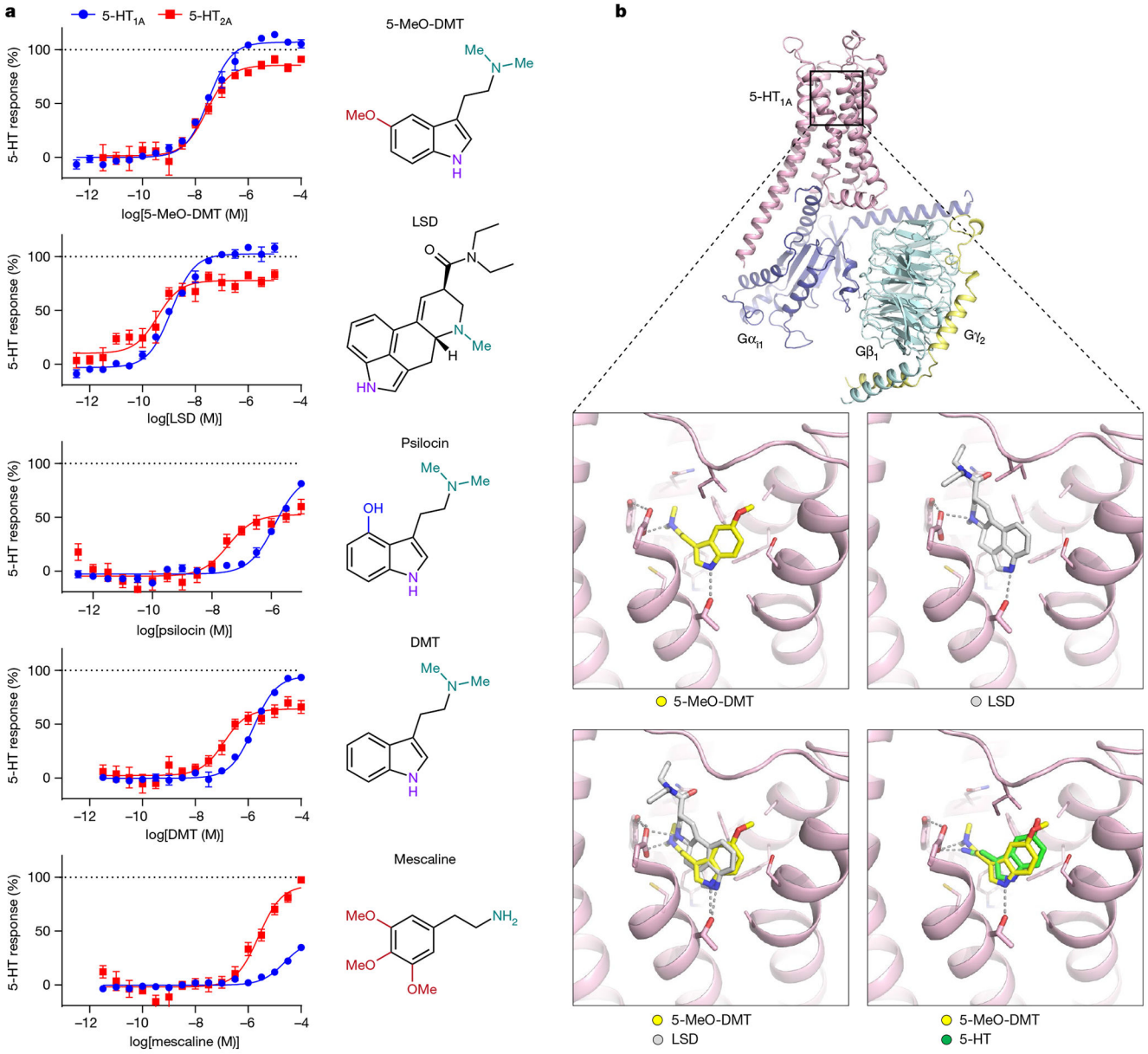

Fig. 1 |. Activity of psychedelics at 5-HT$_{1A}$ and 5-HT$_{2A}$, and cryo-EM structures of 5-MeO-DMT and LSD bound to the 5-HT$_{1A}$ signalling complex.

a, 5-HT$_{1A}$-mediated G$_{i1}$ activation (blue) and 5-HT$_{2A}$-mediated G$_q$ activation (red) by psychedelics determined by BRET. Concentration–response experiments were performed in triplicate and are averaged from two (mescaline) or more (all other compounds) independent experiments. Data are normalized against 5-HT and errors bars denote the s.e.m. **b**, Top, cryo-EM structure of 5-HT$_{1A}$–Gα_{i1}–Gβ_1-Gγ_2 signalling complexes. 5-HT$_{1A}$, Gα_{i1}, Gβ_1 and Gγ_2 are shown in pink, dark blue, teal and yellow, respectively. Middle, zoom-in images show the 5-HT$_{1A}$ orthosteric site bound to 5-MeO-DMT (yellow) and LSD (grey), with ionic interactions and hydrogen bonds indicated by dashed lines. Bottom, superposition of 5-HT$_{1A}$ orthosteric binding sites comparing binding poses of 5-MeO-DMT and LSD, as well as 5-MeO-DMT and 5-HT (Protein Data Bank (PDB) identifier: 7E2Y).

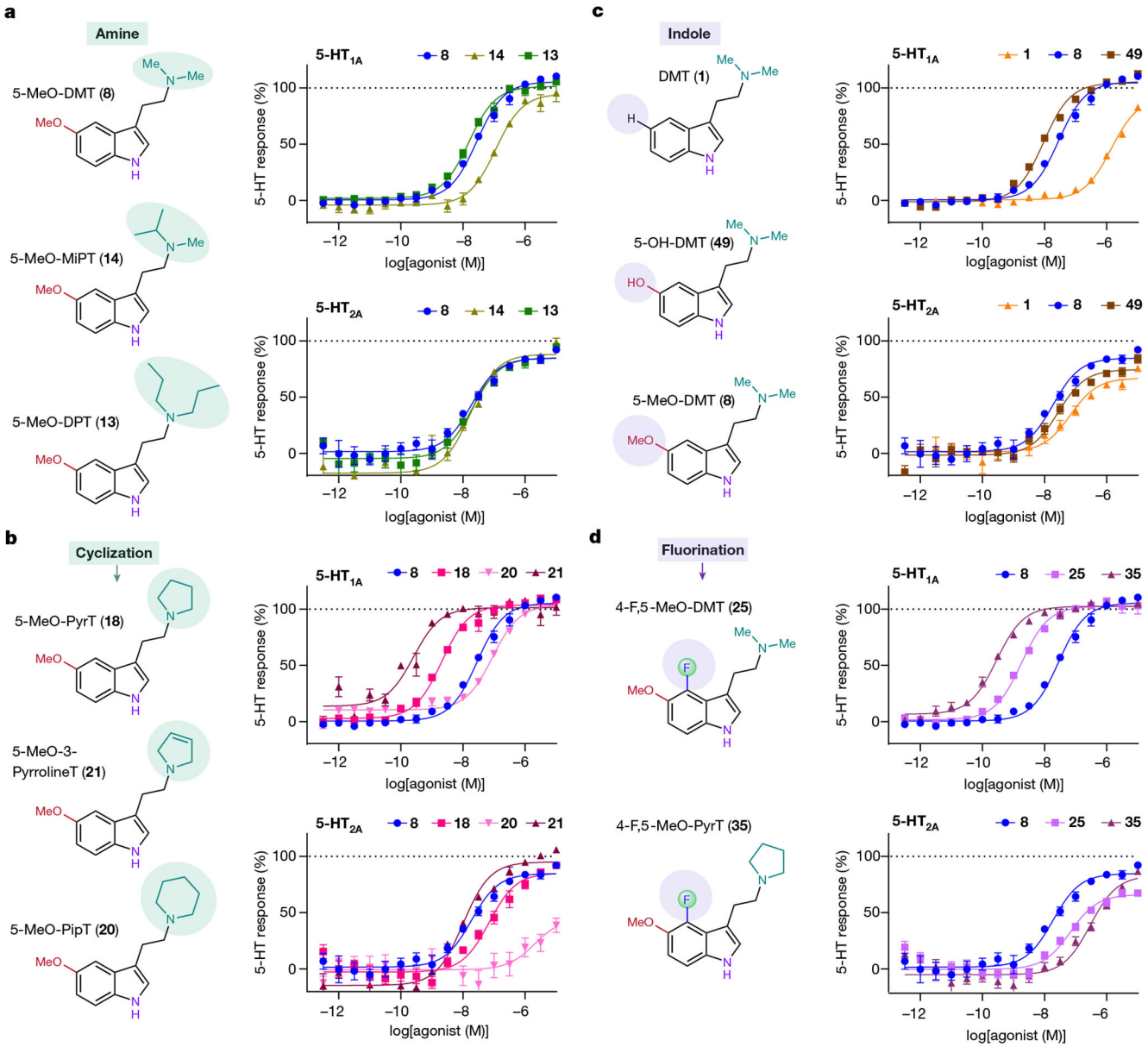

Fig. 2 |. Differential pharmacological effects of amine and indole modifications to the 5-MeO-DMT scaffold at 5-HT$_{1A}$ and 5-HT$_{2A}$.

a,b, Schematic of modifications (left) and 5-HT$_{1A}$–Gi and 5-HT$_{2A}$–G$_q$ BRET concentration–response activity (right) mediated by 'designer' tryptamines (**a**) and cyclized tryptamines **(b). c,d,** Schematic of modifications (left) and effects of indole modifications at the fifth position (**c**) and 4-fluorination (**d**) on 5-HT$_{1A}$–Gi and 5-HT$_{2A}$–G$_q$ BRET activity (right). All signalling experiments were performed in triplicate and are averaged from two (5-MeO-MiPT, 5-MeO-3-PyrrolineT, 5-MeO-PipT) or three (all other compounds) independent experiments. Data are normalized against 5-HT and errors bars denote the s.e.m.

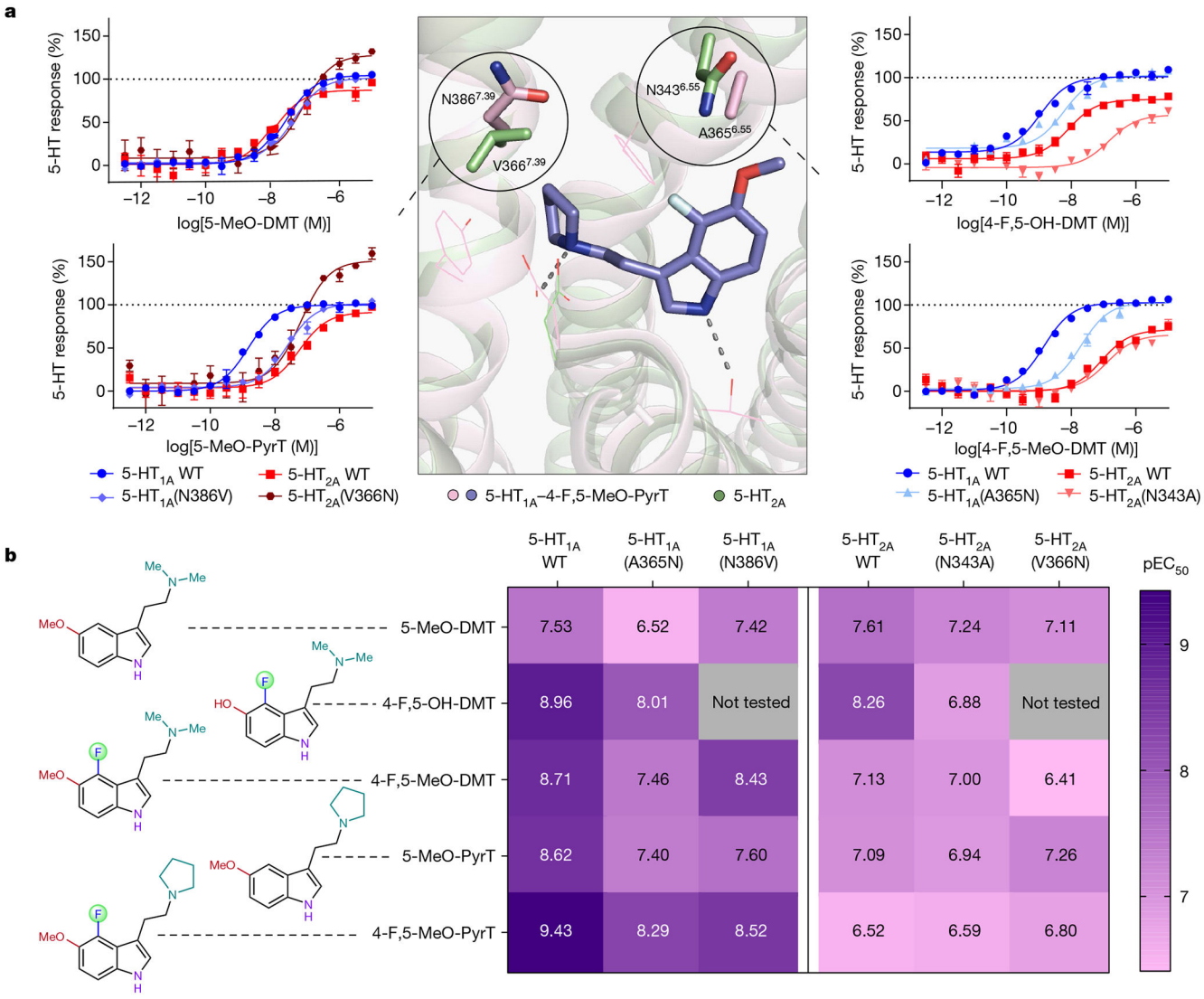

Fig. 3 |. Elucidation of potency and selectivity determinants of tryptamines at 5-HT$_{1A}$ and 5-HT$_{2A}$.

a, Left and right, 5-HT$_{1A}$–G$_i$ and 5-HT$_{2A}$–G$_q$ signalling mediated by tryptamine compounds at mutant and wild-type (WT) receptors according to BRET assays. Middle, residue differences in OBPs of 5-HT$_{1A}$ (pink) and 5-HT$_{2A}$ (green; PDB identifier 6WGT). **b**, Heatmap showing the effect of tryptamine modifications on the signalling potency (pEC$_{50}$) at mutant and wild-type 5-HT$_{1A}$ and 5-HT$_{2A}$ receptors. Grey boxes indicate compound not tested. All signalling experiments were performed in triplicate and are averaged from two (5-HT$_{1A}$(N386V), 5-HT$_{2A}$(V366N), 5-HT$_{1A}$(A365N): 4-F,5-MeO-PyrT; 5-HT$_{2A}$(N343A): 4-F,5-MeO-PyrT) or three (all other compounds) independent experiments. Data are normalized against 5-HT and errors bars denote the s.e.m.

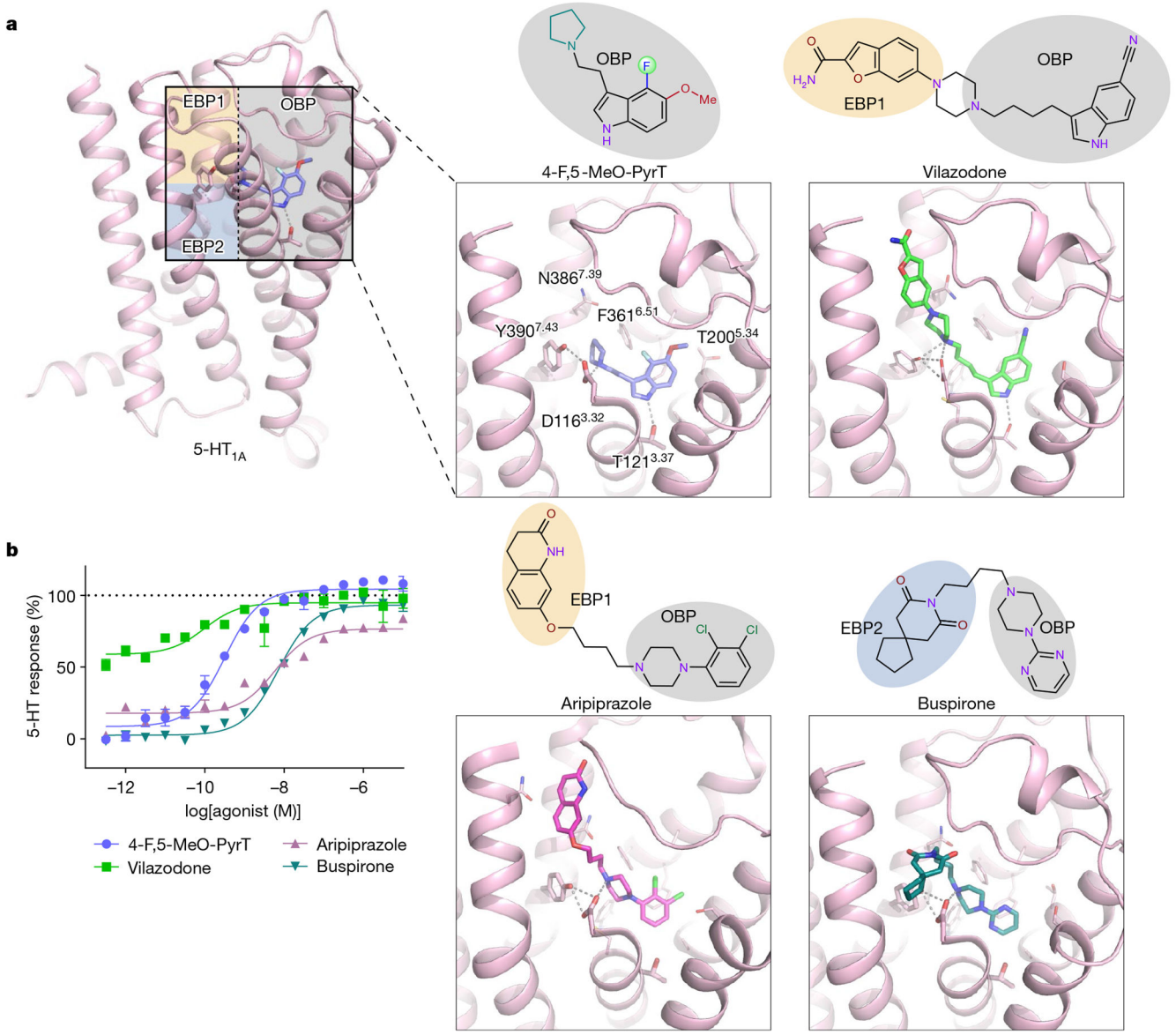

Fig. 4 |. Structural and functional comparison of 4-F,5-MeO-PyrT and clinical 5-HT$_{1A}$ medications at 5-HT$_{1A}$.

a, Top, two-dimensional structures of 4-F,5-MeO-PyrT, vilazodone, aripiprazole and buspirone. Bottom, structural comparison of drug-binding poses of 4-F,5-MeO-PyrT (blue), vilazodone (green) and buspirone (teal) determined in this study, as well as a previous structure of aripiprazole (magenta; PDB identifier 7E2Z). Buspirone assumes a kinked conformation binding to a previously undescribed EBP (EBP2, blue shade), whereas vilazodone and aripiprazole stretch towards the extracellular space forming interactions in a distinct EBP (EBP1, yellow shade). All compounds assume similar overall poses in the OBP (grey shade) of 5-HT$_{1A}$. **b**, 5-HT$_{1A}$–G$_i$ BRET values of 4-F,5-MeO-PyrT, vilazodone, aripiprazole and buspirone. All signalling experiments were performed in triplicate and are averaged from two (aripiprazole) or three (all other compounds) independent experiments. Data are normalized against 5-HT and errors bars denote the s.e.m.

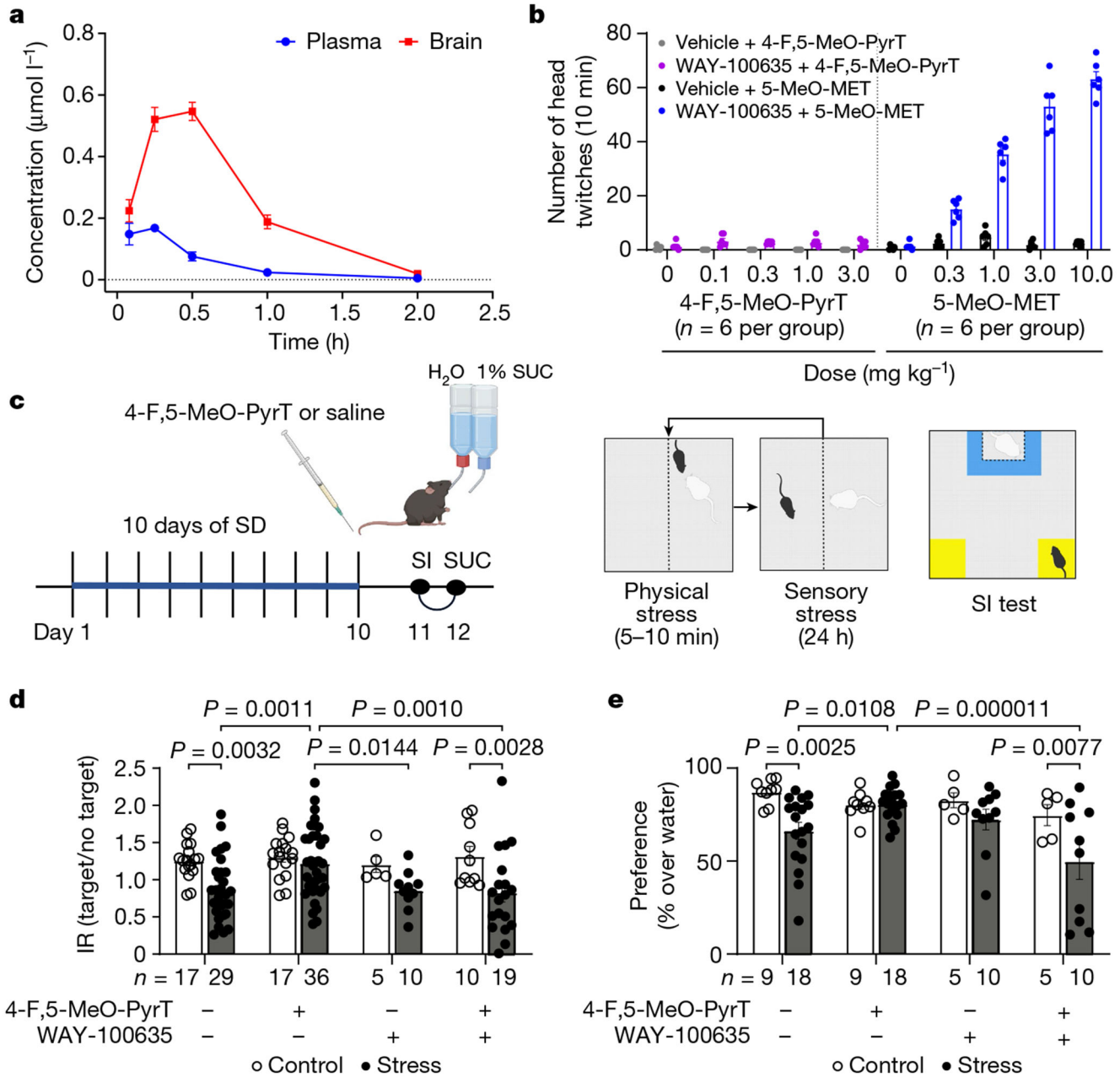

Fig. 5 |. Effects of 5-MeO-DMT derivatives on mouse behaviour.

a, Pharmacokinetics profile of 4-F,5-MeO-PyrT following s.c. administration of 1 mg kg^{-1}. Data were obtained from three mice per time point ($n = 3$). **b**, HTR as a measure of 5-HT_{2A}-mediated hallucinogenic activity in mice in the presence and absence of the 5-HT_{1A}-selective antagonist WAY-100635 (1 mg kg^{-1}). **c**, Schematic of the chronic SD stress paradigm. **d**,**e**, Effects of saline, 4-F,5-MeO-PyrT and WAY-100635 administration on control mice and chronically defeated (stressed) mice. Determination of SI (**d**) and preference for 1% sucrose (SUC) solution over water in a two-bottle choice test (**e**) as a measure of a depressive-like phenotype. Compounds were dosed at 1 mg kg^{-1} unless otherwise indicated. Data are averaged from three (**d**) and two (**e**) independent experiments,

and the number of mice for each group is indicated below the data for each respective group. Differences were determined by two-way analysis of variance with multiple comparisons using Fisher's least significance difference post hoc test, and exact *P* values are denoted in the figure. Error bars denote the s.e.m. Schematic in **c** was created using BioRender (https://www.biorender.com).